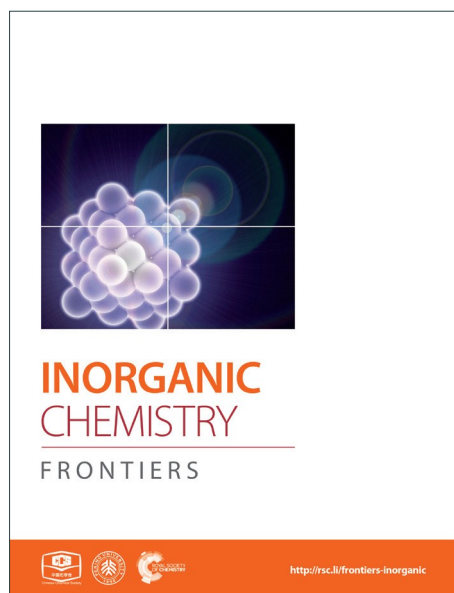
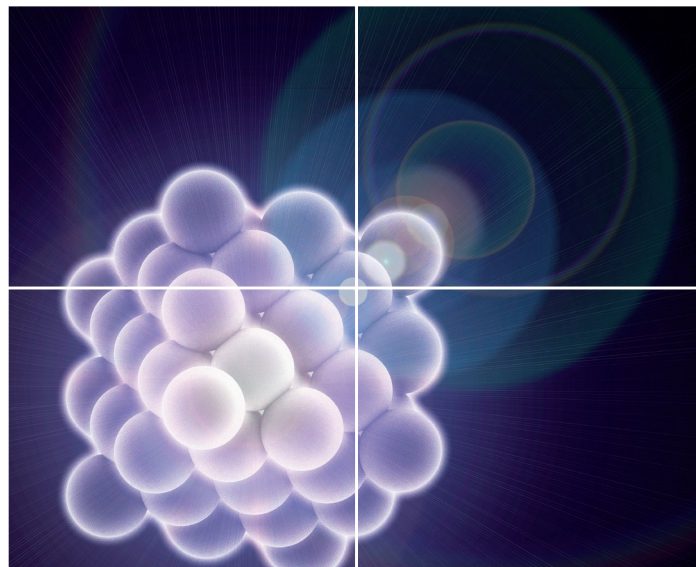


INORGANIC CHEMISTRY

FRONTIERS

Accepted Manuscript



This is an *Accepted Manuscript*, which has been through the Royal Society of Chemistry peer review process and has been accepted for publication.

Accepted Manuscripts are published online shortly after acceptance, before technical editing, formatting and proof reading. Using this free service, authors can make their results available to the community, in citable form, before we publish the edited article. We will replace this *Accepted Manuscript* with the edited and formatted *Advance Article* as soon as it is available.

You can find more information about *Accepted Manuscripts* in the [Information for Authors](#).

Please note that technical editing may introduce minor changes to the text and/or graphics, which may alter content. The journal's standard [Terms & Conditions](#) and the [Ethical guidelines](#) still apply. In no event shall the Royal Society of Chemistry be held responsible for any errors or omissions in this *Accepted Manuscript* or any consequences arising from the use of any information it contains.

Unprecedented formation of organo-ruthenium(II) complexes containing 2-hydroxy-1-naphthaldehyde S-benzoyldithiocarbamate: Synthesis, X-ray crystal structure, DFT study and biological activities *in vitro*

Paranthaman Vijayan,^a Periasamy Viswanathamurthi,^{*a} Paramasivam Sugumar,^b Mondikalipudur Nanjappagounder Ponnuswamy,^b Manickam Dakshinamoorthi Balakumaran,^c Pudupalayam Thangavelu Kalaichelvan,^c Krishnaswamy Velmurugan,^d Raju Nandhakumar^d and Ray Jay Butcher^e

^a*Department of Chemistry, Periyar University, Salem-636 011, India.*

^b*Centre of Advanced Studies in Crystallography and Biophysics, University of Madras, Guindy Campus, Chennai- 600 025, India.*

^c*Centre for Advanced Studies in Botany, School of Life Sciences, University of Madras, Guindy Campus, Chennai - 600 025, Tamil Nadu, India.*

^d*Department of Chemistry, Karunya University, Karunya Nagar, Coimbatore - 641 114, India.*

^e*Department of Chemistry, Howard University, 525 College Street NW, Washington, DC 20059, USA.*

*To whom correspondence should be addressed, e-mail: viswanathamurthi72@gmail.com

Fax: +91 427 2345124

Abstract

As a contribution to the development of new ruthenium complexes with pharmacologically interesting properties, two new mononuclear ruthenium(II) complexes of the general formula $[\text{Ru}(\text{H-Nap-sbdtc})\text{Cl}(\text{CO})(\text{EPh}_3)_2]$ (**1&2**) [H-Nap-sbdtc] = 2-hydroxy-1-naphthaldehyde-S-benzyl-dithiocarbazate; E= P or As] were synthesized. The new ruthenium(II) carbonyl complexes are remarkably stable and were obtained in good yields. Their identities have been established by satisfactory elemental analyses and various spectroscopic techniques (IR, UV/visible, (^1H , ^{13}C , and ^{31}P) NMR, ESI-MS). For better definition, the molecular structure of the complexes **1** and **2** has been determined by X-ray crystallography, which confirm the coordination mode of ligand and reveal a distorted octahedral geometry around the ruthenium ion. The molecular structure of the complexes **1** and **2** has been optimized by DFT calculation. The binding affinity and binding mode of ligand and their ruthenium(II) complexes toward calf thymus CT-DNA were determined by emission spectral method, fluorescent indicator displacement (FID) assay and viscosity measurement. Further, the interactions of the ligand and their complexes **1** and **2** with bovine serum albumin (BSA) were investigated using UV-Vis and fluorescence spectroscopic methods. Absorption and emission spectral studies indicate that the complexes **1** and **2** interact with CT DNA and BSA protein more strongly than their parent ligand. In addition, the interactions of the complexes with DNA/BSA were followed by electrophoretic mobility spectrometry studies and the results show that these complexes exhibited good cleavage properties. *In vitro* anticancer activity has been scrutinized by MTT assay, acridine orange/ethidium bromide (AO/EB) and diamidino-2-phenylindole (DAPI) staining against human cervical cancer (HeLa) cell line.

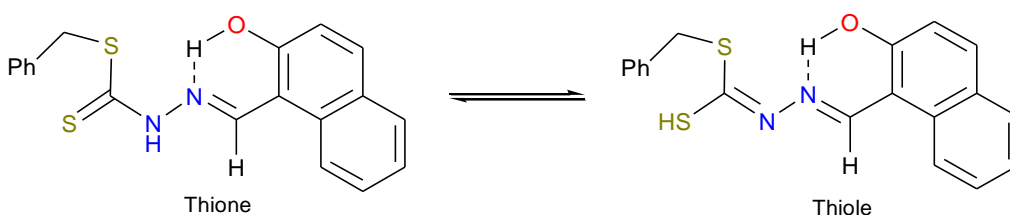
Key words: Ruthenium(II) carbonyl complex, X- ray structure, DFT, DNA/BSA affinities, *In vitro* cytotoxic activities

Introduction

The present challenges of inorganic medicinal chemistry are (a) to improve the therapeutic performance of classic platinum anticancer drugs such as cisplatin, carboplatin and oxaliplatin, based on over 30 years of research and successful clinical use¹ (b) to open a new scenario by investigating the potential activity of metal drugs for the diagnosis and therapy of other pathologies, mainly cancer diseases, where an aberrant biochemistry of endogenous metals seems to have a relevant role.² Nevertheless, there is limited effectiveness due to severe side effects and acquired resistance due to prolonged treatment have spurred investigators to find alternatives metal based drugs.³ Among them ruthenium-based complexes, which exhibit considerable promise in antiproliferation activity and lower toxicity than platinum drugs, have been developed in the last two epochs. In particular, the ruthenium complexes, [HIm][trans-RuCl₄(DMSO)(Im)] (NAMI-A) and [ImH][trans-Ru-Cl₄(Im)₂] (KP1019), have progressed into clinical trials with very promising results.^{4,5} The mechanism of action of these above ruthenium complexes have been widely studied in order to establish the basis for their unique properties, and it would appear that three main features are relevant: first, they interact with serum proteins such as albumin and transferrin that endows them with tumor seeking properties,^{6a} second, ruthenium(III) complexes appear to be activated through intracellular reduction to allow generation of toxic ruthenium(II) species^{6b} and third, at the tumor site reactions (binding) with proteins are preferred to DNA binding, which contrasts with the behavior of platinum(II) complexes such as cisplatin.^{6c} Extrapolation of these pathways led to the direct evaluation of ruthenium(II) complexes.^{6d,e} On the other hand, most of the recent research on anticancer ruthenium(II) compounds has been focused that drugs (metal complexes) not only bind to the primary target DNA, but also strongly interact with serum albumins proteins such as BSA and HSA. It is essential to explore drug-protein interactions as most of the drugs bound to serum albumin are usually transported as a protein complex. Attention has also been focused on the proteins that drive and control cell cycle progression.⁷ Therefore, development of the anticancer agents targeting both DNA and BSA proteins are highly sought after.

Schiff bases derived from S-alkyl/aryl esters of dithiocarbazic acid have backbones similar to those of thiosemicarbazones, differing only in the terminal non-coordinating functional group attached to the thiocarbonyl moiety. Metal chelates of dithiocarbazic acid derivatives represent a class of organic compounds that have been explored because of their broad spectrum

of biological activities.⁸ Although the synthesis of S-benzylthiocarbazates and its derivatives have been under study for many years, considerable attention continues to be given to their metal complexes, since their properties can be greatly modified by introducing different substituents.⁹ The presence of nitrogen and sulfur atoms as medium and low crystal-field donors (hard–soft ligands), gives dithiocarbazates good ability to coordinate metal ions, yielding metal complexes with interesting structural and electronic properties.¹⁰ In S-substituted dithiocarbazate compounds, owing to thione–thiol tautomer (Scheme 1), N and S donor atoms were linked to the metal ion with the construction of five- or six-membered rings.^{11,12} The coordination of S-benzylthiocarbazate to ruthenium ion, hopefully give better bio active performance.



Scheme 1 Thione and thiol forms of 2-hydroxy-1-naphthaldehyde-S-benzylthiocarbazate [H_2 -(Nap-sbdtc)]

In this paper, we have described two new organo-ruthenium complexes comprising naphthaldehyde based dithiocarbazates, as shown in Scheme 2, together with DFT study and their binding ability towards calf thymus (CT) DNA/BSA protein. Furthermore, their manifest cytotoxic activity towards normal Vero cell line and HeLa (human cervical cancer) cell line is evaluated using MTT assay and cell death analysis by AO/EB and DAPI staining.

Experimental section

Materials

The dithiocarbazate ligand [H_2 -(Nap-sbdtc)] was synthesized according to previously published method with slightly modification.^{13a} The ruthenium precursor [$\text{RuHCl}(\text{CO})(\text{EPh}_3)_3$] [E= P or As] were synthesized based on the standard procedures.^{13b} All synthetic manipulations were routinely performed under oxygen atmosphere. All the reagents used in this study were reagent grade and used without further purification. Solvents were purified and dried according to the standard procedures. Doubly distilled water was used to prepare buffers. Calf thymus DNA (CT-DNA), agarose, protein markers and Bovine serum albumin (BSA) were obtained from Genei, Bangalore and Himedia, India respectively. $\text{RuCl}_3 \cdot 3\text{H}_2\text{O}$, Ethidium bromide (EB), Methylene

blue, Tris(hydroxymethyl) amino methane were purchased from Sigma-Aldrich and used as received.

General methods

Elemental analyses (C, H, N and S) were carried out on a Vario EL III CHNS analyzer at SAIF-Cochin, India. Infrared spectra were recorded as KBr pellets using a Perkin-Elmer FT-IR spectrophotometer in the range 4000-400 cm^{-1} . ^1H and ^{13}C NMR spectra were measured on a Bruker Ultra Shield at 300 MHz using CDCl_3 as solvent and TMS as an internal reference. Mass spectra for the complexes were recorded on an advanced Q-TOF microTM mass spectrometer using electrospray ionization probe. Electronic spectra have been obtained on a JASCO V-570 spectrophotometer. Geometry optimization by density functional theory (DFT) method were performed using the GAUSSIAN09 (B3LYP/LANL2DZ) package. Fluorescence spectral data were performed on a JASCO FP-8200 fluorescence spectrophotometer at room temperature. Gel electrophoresis was carried out by Bio-rad UV Transilluminator and their image has taken by Sony cyber shot WX60. Single crystal X-ray diffraction data collections were carried out at 173 K on a Bruker Apex-II CCD diffractometer equipped with a liquid nitrogen cryostat. The melting points were checked on a technico micro heating apparatus and are uncorrected. Stock solutions of ruthenium(II) complexes (1.0×10^{-3} M in DMSO) were stored at 4°C and required concentrations prepared for all experiments. All the stock solutions used after no more than four days. Solutions of compounds were freshly prepared 1 hour prior to biochemical evaluation. Data were expressed as the mean \pm the standard deviation from three independent experiments.

Synthetic procedure for new ruthenium(II) complexes

A solution of [H_2 -(Nap-sbdtc)] (0.029 g; 0.1 mmol) in 20 ml of MeOH/ CHCl_3 (1:1 v/v) was added drop wise to a boiling solution of [$\text{RuHCl}(\text{CO})(\text{EPh}_3)_3$] (E= P or As) (0.100 g; 0.1 mmol) in MeOH/ CHCl_3 solvent mixture (1:1 v/v) (20 ml). The mixture was gently heated under reflux for 8 hours resulted in a rapid change of color from light orange to dark red (maroon). The reaction was monitored by thin-layer chromatography (TLC) using a silica gel on aluminum sheets with 20/80 mixture of ethyl acetate/pet ether as the mobile phase. After refluxing, the resulting solution was filtered and the filtrate was left unperturbed for the slow evaporation of the solvent. After four days yellowish orange colored big crystals suitable for X-ray diffraction were obtained.

Characterization data. [Ru(H-Nap-sbdtc)(CO)Cl(PPh₃)₂] (**1**). Yield: 65% (0.55 mg); Color: Orange; MP: 215-220°C; Micro analytical data: C₅₆H₄₅ClN₂O₂P₂RuS₂ requires: C, 64.64; H, 4.36; N, 2.69; S, 6.16 Found: C, 64.21; H, 4.02; N, 2.50; S, 6.01%; IR (KBr pellet, cm⁻¹) 3386 ν(-OH); 1606 ν(C=N); 1290 ν(C-O), 771 ν(C-S), 1952 ν(C≡O), 1064 ν(N-N), 1442 ν{Ph(P-Ph)}; UV-vis (CHCl₃), λ_{max} (nm): 261, 338, 382, 408, 427. ¹H NMR (300.13 MHz, CDCl₃, ppm): 3.90 (s, 2H, -CH₂); 8.84 (s, 1H, -CH=N); 9.19 (s, 1H, -OH); 6.97-7.78 (m, 11H, Ar); ¹³C NMR (300.13 MHz, CDCl₃, ppm): 204.04 (C≡O), 185.42 (C-S), 159.56 (-CH=N), 151.81 (C-O), 134.54 (Ar C), 134.25 (Ar C), 133.96 (Ar C), 133.83 (Ar C), 133.74 (Ar C), 133.66 (Ar C), 133.10 (Ar C), 132.80 (Ar C), 132.51 (Ar C), 132.01 (Ar C), 134.54 (Ar C), 129.42 (Ar C), 129.35 (Ar C), 128.91 (Ar C), 128.67 (Ar C), 128.49 (Ar C), 128.16 (Ar C), 128.08 (Ar C), 127.88 (Ar C), 127.82 (Ar C), 127.76 (Ar C), 127.67 (Ar C), 127.63 (Ar C), 127.11 (Ar C), 126.85 (Ar C), 126.73 (Ar C), 122.74 (Ar C), 122.01 (Ar C), 118.46 (Ar C), 118.28 (Ar C), 34.76 (-CH₂); ³¹P NMR (162 MHz, DMSO-d₆, ppm) 32.13; ESI-MS (Calcd, found, m/z) = 1005.1, 1005.4 (M-Cl)⁺. Single crystals suitable for an X-ray determination were grown by slow evaporation of methanol-chloroform (1:1 v/v) solution of **1** at room temperature.

[Ru(H-Nap-sbdtc)(CO)Cl(AsPh₃)₂] (**2**). Yield: 61% (0.52 mg); Color: Orange; MP: 222-228 °C; Micro analytical data: C₅₆H₄₅As₂ClN₂O₂RuS₂ requires: C, 59.60; H, 4.02; N, 2.48; S, 5.68. Found: C, 54.32; H, 3.92; N, 2.13; S, 5.47%; IR (KBr pellet, cm⁻¹) 3382ν(-OH); 1601 ν(C=N); 1282 ν(C-O), 779 ν(C-S), 1961 ν(C≡O), 1072 ν(N-N), 1433 ν{Ph(As-Ph)}; UV-vis (CHCl₃), λ_{max}(nm): 266, 342, 370, 400, 432; ¹H NMR (300.13 MHz, CDCl₃, ppm): 3.95 (s, 2H, -CH₂); 9.14 (s, 1H, -CH=N); 11.42 (s, 1H, -OH); 6.78-7.65 (m, 11H, Ar); ¹³C NMR (300.13 MHz, CDCl₃, ppm) 203.82 (C≡O), 184.83 (C-S), 158.22 (-CH=N), 150.81 (C-O), 136.69 (Ar C), 133.56 (Ar C), 133.43 (Ar C), 133.35 (Ar C), 132.96 (Ar C), 132.22 (Ar C), 132.16 (Ar C), 129.30 (Ar C), 128.60 (Ar C), 128.37 (Ar C), 128.25 (Ar C), 128.11 (Ar C), 127.87 (Ar C), 127.46 (Ar C), 127.18 (Ar C), 126.87 (Ar C), 122.82 (Ar C), 121.88 (Ar C), 118.22 (Ar C), 108.98 (Ar C), 34.79 (-CH₂); ESI-MS (Calcd, found, m/z) = 1093.0, 1093.5 (M-Cl)⁺. Single crystals suitable for an X-ray determination were grown by slow evaporation of ethanol-dichloromethane (1:1 v/v) solution of **2** at room temperature.

X-ray structure determination

Suitable single crystals of the complexes **1** and **2** were mounted on a glass fibers with epoxy cement. The crystals were cut into a fitting size (less than collimator cross section diameter). The crystal data collections were performed with an automated Xcalibur, Ruby, Gemini at 123(2) and Bruker SMART APEX 2 at 296(2) CCD diffractometer using graphite monochromatized Mo (K α) ($\lambda = 0.71073$ Å). The data were corrected for Lorentz and polarization effects with the SMART¹⁴ suite programs and for absorption effects with SADABS. A data collection strategy using ω and ϕ scans at 0.5° scan technique yielded full hemispherical data with excellent intensity statistics. Structure solutions and refinements were performed by the programs SHELXS-97¹⁵ and SHELXL-13. The structures were solved by direct methods to locate the heavy atoms, followed by difference maps for the light non-hydrogen atoms. Anisotropic thermal parameters were refined for the rest of the non-hydrogen atoms. Hydrogen atoms were placed geometrically and refined isotropically. Crystal data and experimental details for the crystal **1** and **2** were shown in Table 2.

Computational method (DFT)

All computations were performed using the GAUSSIAN09 (G09) program. Full geometry optimizations of the complexes **1** and **2** were carried out using the DFT method at the Becke's three-parameter hybrid exchange functional (B3LYP) level of theory.¹⁶ This functional has been shown to give more accurate results for organometallic complexes. The metal atom was described using the Lee–Yang–Parr nonlocal correlation functional (LANL2DZ) basis set while all the non-metal atoms were described using the 6-31G* basis set. Gauss Sum was used to calculate the fractional contributions of various groups to each molecular orbital. A difference between the experimental and theoretical studies is that computations were done in the gas phase, whereas the X-ray data was obtained in the solid phase for complexes. Geometry optimizations have been done without any symmetry restriction by X-ray coordinates of the molecule. Frequencies of all complexes have been computed at the same level of theory to confirm that all optimized structures are at true minima, which means they have no imaginary frequencies. At the same level and basis sets, calculations of natural electron population, natural charge for each atom and frontier molecular orbitals of the complexes have been performed by natural bond orbital (NBO) analysis on the gas phase optimized structures.¹⁷ The molecular

orbital plots have been generated using the Chemcraft program package (<http://www.chemcraftprog.com>).

DNA interaction studies

Flourescence titration for DNA binding

DNA binding experiments include emissive spectral traces and viscosity measurement conformed to the standard methods and practices previously implemented by our laboratory. The reported compounds were not soluble in water in titration conditions. So the stock solutions of selected test compounds were dissolved in mixed solvent of 5% DMSO and 95% Tris-HCl buffer (5mM Tris-HCl / 50mM NaCl buffer for pH-7.2) for all the experiments and stored in 4° C for further use. The solvent medium has no influence over the compounds. While measuring the emissive spectra, an equal amount of DNA was added to the test compound solutions and the reference solution to eliminate the absorbance of the CT-DNA itself and Tris-HCl buffer was subtracted through base line correction. The excitation wavelength was fixed by the emission range and adjusted before measurements. Emissive titration experiments were performed with a fixed concentration of the solution of ligand and their metal complexes (25 μ M). While gradually increasing the concentration (0-30 μ M) of DNA, the emission intensities were recorded at 425 nm (λ_{ex}) in the range of 430-700 nm. Titrations were manually done by using a micropipette for the addition of CT-DNA. It is noteworthy here that the DNA in double distilled water does not show any luminescence.

Ethidium bromide displacement study

DNA binding propensity of ligand [H_2 -(Nap-sbdtc)] and their ruthenium complexes were measured by the fluorescence-based ethidium bromide displacement. A typical assay was carried out as follows. Ethidium bromide (EB) displacement experiments were performed by monitoring changes in the fluorescence intensity on the emission wavelength λ_{em} 602 nm at the excitation wavelength of λ_{ex} 500, after aliquot addition of tested compounds to an aqueous solution of the EB-DNA. EB alone showed minimal fluorescence and the fluorescence was enhanced greatly with gradual addition of CT DNA until maximum fluorescence was achieved due to the formation of an intercalative DNA-EB adduct. Addition of increasing amounts of the ruthenium complex to the DNA-EB adduct quenched the fluorescence. For the emission quenching

experiments, CT-DNA was pretreated with EB in the ratio $[DNA] / [EB] = 10$ for 30 minutes at 37°C . Then the titration compounds were added to this mixture of EB-DNA and the change in the fluorescence intensity was measured.

Viscosity experiment

Viscosity measurements were carried out using an Ubbelodhe viscometer maintained at a constant temperature of 30.0°C (± 0.1) in a thermostatic bath. DNA samples of approximately 200 base pairs in length were prepared by sonication in order to minimize complexities arising from CT-DNA flexibility. The flow time was measured three times, after 5 min of incubation, with each addition of the ligand and their complexes and the average flow time was taken for calculation of relative viscosity. Relative viscosities for CT-DNA in the presence and absence of the compound were calculated from the relation $g = (t - t_0)/t_0$, where t is the observed flow time of DNA-containing solution and t_0 is the flow time of Tris-HCl buffer alone. Data were presented as $(\eta/\eta_0)^{1/3}$ versus binding ratio ($R = [Ru] / [DNA] = 0.0-1.2$), where η is the viscosity of CT-DNA in the presence of the compound, and η_0 is the viscosity of CT-DNA alone.

Gel electrophoresis shift assay

DNA cleavage experiments were carried out using supercoiled pBR322 DNA using agarose gel electrophoresis. Stock solutions of DNA were diluted using milli-Q water and solutions of the ligand and their ruthenium(II) complexes **1** and **2** ($25\ \mu\text{M}$) were prepared in freshly made $20\ \text{mM}$ Tris-HCl buffer at $\text{pH}-7.2$. Reactions were performed by incubating the DNA, in the absence/presence of increasing concentrations of the compounds at 37°C . After 4 h incubation, the reaction mixture was quenched by adding $4\ \mu\text{L}$ of loading dye ($10\ \text{mM}$ Tris-HCl, $0.1\ \text{M}$ EDTA, 0.25% bromophenol blue) and then frozen at -20°C for 30 min. The reaction mixture was loaded on the agarose gel (0.9%), and the electrophoresis was carried out in a dark room at $50\ \text{V}$ for 3 h in TAE buffer ($40\ \text{mM}$ Tris base, $20\ \text{mM}$ acetic acid, $1\ \text{mM}$ EDTA). Agarose gel was stained with ethidium bromide solution ($1\ \mu\text{g}/\text{mL}$) for 30 min followed by destaining for 4 h in milli-Q water.¹⁸ The efficiency of new compounds for the conversion of supercoiled DNA (SC) Form I to Form II (NC) and then to form III (linear form) i.e, produced when both strands are broken was measured. Cleaved DNA bands were visualized under UV light and photographed.

Bovine serum albumin interaction studies

BSA binding

Quenching of the tryptophan residues of BSA was performed using ligand [$\text{H}_2\text{-(Nap-sbdtc)}$] and their ruthenium complexes **1** and **2** as quenchers. Quenching of the emission intensity of tryptophan residues of BSA at 344 nm (excitation wavelength at 280 nm) was monitored using selected compounds as quenchers with increasing compound concentration. Titrations were manually done by using a micropipette for the addition of test compounds. The Stern–Volmer (2) and Scatchard (3) equations and graphs may be often used in order to study the interaction of the quencher with BSA.

BSA photo cleavage

Protein cleavage experiments were carried out by incubating BSA (4 μM) with selected test compounds (50 μM) in Tris-HCl buffer for 4 h at 37 $^\circ\text{C}$ according to the literature.¹⁹ The samples were dissolved in the loading buffer (24 μL) containing SDS (7% w/v), glycerol (4% v/v), Tris-HCl buffer (50 mM, pH 6.8), mercaptoethanol (2% v/v) and bromophenol blue (0.01% w/v). The protein solutions were then denatured on heating to boil for 3 min. The samples were then loaded on a 3% polyacrylamide (stacking) gel. Gel electrophoresis was done initially at 60 V until the dye passed into the separating gel (12% polyacrylamide) from the stacking (3%) gel, [separating gel/stacking gel concentration 4.05/2.75 mL distill water, 2.5/1.7 mL tris buffer (pH- 8.8/6.8), acromade 3.3/2.3 mL, SDS 250/100 μL , APS 250/100 μL , Temed 75/50 μL] followed by setting the voltage to 110 V for 1.5 h. Staining was done with CBR-250 (Coomassie brilliant blue R-250) solution (acetic acid-methanol-water = 1:2:7 v/v) and destaining were done with water-methanol-acetic acid mixture (5:4:1 v/v) for 4 h. The gels, after destaining were scanned and the images were photographed.

MTT assay

Maintenance of cancer cell lines

The HeLa (human cervical cancer) cell line was obtained from National Centre for Cell Sciences Repository, University of Pune, India. Vero and HeLa cells were maintained in a humidified atmosphere containing 5% CO_2 at 37 $^\circ\text{C}$ in *Dulbecco's modified Eagle's* medium (DMEM)

supplemented with 100 units of penicillin, 100 $\mu\text{g mL}^{-1}$ of streptomycin and 10% fetal bovine serum (FBS). Briefly, Vero and HeLa cells were precultured in 96-well microtiter plates for 48 h under 5% CO_2 .

Preparation of samples for cell line testing

The compounds were dissolved in 0.1% DMSO (the concentration of DMSO did not exceed 0.1% v/v) to obtain a solution of 1 mM each. The samples were then diluted to 100 μM in PBS solution and filter-sterilized using a 0.22 μm syringe filter. This 100 μM solution in PBS was further used in cell cytotoxicity studies. The cells (1×10^6 cells/mL per well) were seeded in a 96-well plate. One day after seeding, the cells were treated with or without different concentration of test compounds and re-incubated at 37 $^\circ\text{C}$ in a CO_2 incubator for 24 h. After the incubation, the cells were visualized using an inverted Olympus microscope.

Protocol for MTT assay

The effect of ligand and their ruthenium(II) complexes on Vero and HeLa cells viability was determined by 3-(4,5-dimethylthiazol-2-yl)-2,5-diphenyltetrazolium bromide (MTT) assay.²⁰ The selected compounds were added to the micro wells containing the cell culture at final concentrations of 5-50 μM . Then each well was loaded with 10 μL MTT solution (5 mg mL^{-1} in PBS pH = 7.4) for 4 hour at 37 $^\circ\text{C}$. The purple formazan crystal was dissolved in 200 μL DMSO, and the cell viability was determined by calculating the absorbance of each well at 540 nm using a BIORAD ELISA plate reader. All experiments were performed in triplicate, and the percentage of cell viability was calculated according to the following equation.

$$\text{Inhibition rate (IR \%)} = \frac{\text{OD (control)} - \text{OD Drug treated cells}}{\text{OD (control)}} \times 100.$$

The IC_{50} values were determined by nonlinear regression analysis using Origin 6.0 software.

AO/EB and DAPI staining

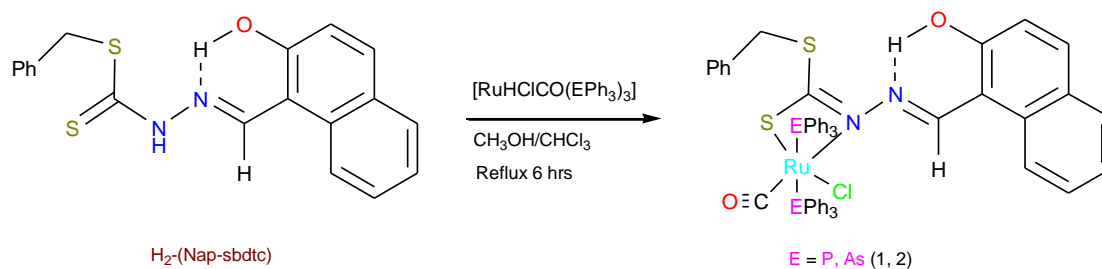
The HeLa cells (1×10^6 in number) were cultured in 6 well plates at 37 $^\circ\text{C}$ in an incubator with increasing concentration of the complexes **1** and **2** (50 μM) for 24 h. The cells were harvested and washed with ice-cold phosphate-buffered saline (PBS) and 40 μL of AO/EB solution (1 part of 100 $\mu\text{g/mL}$ of AO in PBS; 1 part of 100 $\mu\text{g/mL}$ of EB in PBS) was added. After staining the cells were washed with PBS twice, suspended in 200 μL of PBS, and the nuclear morphology were observed under a fluorescence microscope in less than 20 minutes. For DAPI staining, the treated cells were fixed with 80% ethanol at room temperature for 30 min. The fixative was removed and the cells were washed with PBS for 3 times, and then incubated with DAPI (1

$\mu\text{g/mL}$) for 45 min at room temperature in the dark. Both techniques were used to distinguish viable cells, early apoptotic cells with blebbing, and necrotic cells. Acridine orange intercalates into the DNA and gives a green fluorescence and thus the viable cells appear with a green nucleus while early apoptotic cells with a condensed or fragmented nuclei. EB is taken up only by the non-viable cells giving a bright orange nucleus of the dead cells overwhelming the acridine orange stain. DAPI dye is effective for fixed-cell staining and quantitation of DNA content. The HeLa cells were mounted on a slide, and the images were observed under a fluorescent microscope in green/blue filter with excitation at 350 nm and emission at 460 nm.

Results and discussion

Synthesis and characterization

We have relied on the use of the stable starting materials $[\text{RuHClCO}(\text{EPh}_3)_3]$ ($\text{E} = \text{P}$ or As) during the synthesis of our ruthenium(II) carbonyl complexes. The dithiocarbazate ligand $[\text{H}_2\text{-(Nap-sbdtc)}]$ were synthesized via the typical condensation route from their parent *S*-benzylidithiocarbazate and 2-hydroxy-1-naphthaldehyde. Successively, the complexes **1** and **2** were prepared via refluxing the equimolar amount of $[\text{H}_2\text{-(Nap-sbdtc)}]$ with $[\text{RuHCl}(\text{CO})(\text{EPh}_3)_3]$ ($\text{E} = \text{P}$ or As). In this reaction, the ligand $\text{H}_2\text{-(Nap-sbdtc)}$ acted as a monobasic bidentate ligand with NS fashion replacing a hydride and a triphenylphosphine/triphenylarsine ligands from the corresponding starting complexes and resulted in a rapid change of color from light orange to dark red (maroon). The slow evaporation of subsequent solution afforded red crystalline ruthenium(II) carbonyl complexes $[\text{Ru}(\text{H-Nap-sbdtc})(\text{CO})\text{Cl}(\text{PPh}_3)_2]$ (**1**) and $[\text{Ru}(\text{H-Nap-sbdtc})(\text{CO})\text{Cl}(\text{AsPh}_3)_2]$ (**2**). (Scheme 2).



Scheme 2 Synthetic strategy of the complexes described in this work. Unprecedented coordinating groups are shown in distinct colors.

The complexes under investigation are crystalline and non-hygroscopic solids, air-stable in solution and in the solid state at room temperature; soluble in common organic solvents such

as methanol, ethanol, benzene, chloroform, dichloromethane, acetone, dimethylsulfoxide, dimethylformamide, and insoluble in hexane, petroleum ether, and diethyl ether. These have been characterized by satisfactory elemental analyses, ESI-MS, IR, NMR (^1H , ^{13}C , ^{31}P) and UV-vis spectral studies. In addition, the structure of the complexes **1** and **2** were confirmed by single crystal X-ray crystallography.

Spectroscopic studies

IR spectra of free ligand were compared with new ruthenium(II) complexes in order to confirm the significant indications regarding coordination of dithiocarbazate. No attempt has been made to assign each individual band to a specific vibration. However the IR spectrum of **H₂-(Nap-sbdtc)** exhibited many intense bands at 3394, 1621 and 817 cm^{-1} corresponding to (ν_{OH}), ($\nu_{\text{C=N}}$) and ($\nu_{\text{C=S}}$) respectively. In the IR spectra of the new complexes, the absorption of broad signal at 3394 cm^{-1} due to the uncoordinated phenolic $-\text{OH}$ group was observed in the complex **1** and **2**. This may be due to the formation of intra molecular hydrogen bonding between phenolic $-\text{OH}$ and either N1 nitrogen atom.²² A sharp band at 1601 and 1609 cm^{-1} corresponding to the azomethine $\nu_{\text{C=N}}$ group, which has been lowered by 20–12 cm^{-1} in the complexes, indicating the coordination of the azomethine nitrogen group bound to the ruthenium atom. Furthermore, a strong band appeared at 818 cm^{-1} in the spectra of the ligand is indicative of $\nu_{\text{C=S}}$. This band was completely disappeared in the new complexes and a new band appeared at 771 and 779 cm^{-1} in the form of $\nu_{\text{C-S}}$ can be attributed to negative coordination of the ligands and ruthenium metal atom, indicating the tautomerism of the $-\text{NH}-\text{C}=\text{S}$ group and subsequent coordination of thiolate sulfur after deprotonation.^{23a} The parallel properties were witnessed in other dithiocarbazate compounds such as S-methyl dithiocarbazates.^{23b} All the complexes display a medium to strong band in the region 1962–1945 cm^{-1} , which is attributed to the terminally coordinated carbonyl group ($\text{C}\equiv\text{O}$) and is observed at a slightly higher frequency than in the precursor complexes.²⁴

The UV-Vis spectra of the complexes recorded in chloroform showed intense absorption and in the near ultraviolet region and they displayed four bands in the region around 261–432 nm. The electronic spectra of the complexes **1** and **2** showed two bands in the 261 and 265 nm regions which can be assigned to intra-ligand transitions in the complexes. The lowest energy absorption maxima located in the 338–408 nm range may be assigned to an $\text{S}(\text{p}\pi)\rightarrow\text{Ru}(\text{d}\pi)$ LMCT transition caused by the promotion of the electron from the full HOMO of the ligand, of

primarily sulfur $p\pi$ character, to the empty LUMO of ruthenium $d\pi$ character.²⁵ The bands at 426-431 nm can be designated as forbidden ($d \rightarrow d$) transition bands of a spin-paired d^6 species with a distorted octahedral structure (Fig. S2A). As shown in Figure 1B, the emission spectra of complexes **1** and **2** recorded in DMSO showed a shoulder peak at 450 nm in Fig. S2B when excited at 426 nm.

The clearest characterization of the synthesized compounds can be seen from the ^1H and ^{13}C NMR spectra for complexes **1** and **2** were summarized in the experimental section, and resulting spectra depicted through Supporting Information. The ^1H NMR spectrum of the ligand showed a singlet at 10.81 ppm is due to $-\text{N}_2-\text{H}-\text{C}=\text{S}$ group. In complexes **1** and **2**, there was no detectable resonance attributable to $-\text{N}_2\text{H}$, supporting coordination of enolization and the thiolate sulphur of the ligand under the anionic form upon deprotonation at N(2).²⁶ In addition, a sharp singlet observed at 11.31 ppm corresponding to phenolic $-\text{OH}$ group in the free ligand has appeared at 11.41–11.42 ppm in both complexes indicating the non-participation of phenolic oxygen in coordination (Fig. S3, S4).²² In addition, the complexes showed a sharp singlet for the azomethine ($-\text{H}-\text{C}=\text{N}_1$) proton at 9.14 and 8.84 for complexes **1** and **2**. The methylene protons of the ligand and complexes **1** and **2**, appearing at 4.01, 3.90, 3.95 ppm respectively, indicate that the S-benzyl sulfur is not involved in coordination.²⁷ The multiple protons of the aromatic ring moiety of the ligands and metal complexes were observed as multiplets in the range of 6.78-7.78 ppm.

The ^{13}C NMR spectra show the expected signals in the appropriate regions. For the uncoordinated dithiocarbazates, the $\text{C}=\text{N}$ and $\text{C}=\text{S}$ signals of dithiocarbazate residues appear in the regions around 146.56 and 196.44 ppm respectively. Upon coordination and formation of complexes, a downfield shift is observed for the ^{13}C NMR signals of the $\text{C}=\text{N}$ (around 12 ppm), while $\text{C}=\text{S}$ carbon signals appeared upfield region at 184.83 and 185.42 for complex **1** and **2** respectively.²⁸ These are consistent with unprecedented N, S coordination and thio-enolization of the $\text{C}=\text{S}$ of dithiocarbazate moieties. In both complexes, aromatic carbon atom of the phenoxy group observed at 151.81 ppm (complex **1**) and 150.81 ppm (complex **2**) are comparable to the literature values.²⁶ The $\text{C}\equiv\text{O}$ carbon resonating at 204.04 (**1**) and 203.82 ppm (**2**) is comparable with earlier observations. In addition the S- CH_2 carbon atom in S-benzyl group showed a signal at 34.76 (**1**) and 34.79 ppm (**2**) respectively (Fig. S5).²⁹

The coordination of triphenylphosphine ligand and their configuration in the new complexes have been confirmed by the ^{31}P NMR spectra. The appearance of only one sharp singlet at 32.13 ppm in complex **1** suggested the presence of two magnetically equivalent triphenylphosphines *trans* to each other (Fig. S6).²⁴ Furthermore, ESI-MS data (in the positive-ion mode) for complexes **1** and **2** have been listed in the experimental section. The ESI-MS analysis of complexes **1** and **2** show most abundant peaks at m/z 1005.4, 1093.5 respectively were assigned to $[\text{M}-\text{Cl}]^+$ ions revealing that the identity of the complexes retained in solution. The observed isotopic distributions and their simulation patterns are in agreement with the assigned formulations, as shown in Fig.S7

Description of the crystal structure of complexes 1 and 2

To gain insight into the coordination chemistry and structural parameters of these complexes **1** and **2** were isolated as good quality single crystals by slow evaporation of a concentrated MeOH/ CHCl_3 solution and characterized by X-ray diffraction. Details about the data collection, solution, and refinement are gathered in the experimental section and Table 1. The ORTEP view of the molecular structure along with a partial atom numbering scheme is shown in Fig. 1, 2 and important bond lengths and angles for the ruthenium(II) complexes are summarized in Table 2.

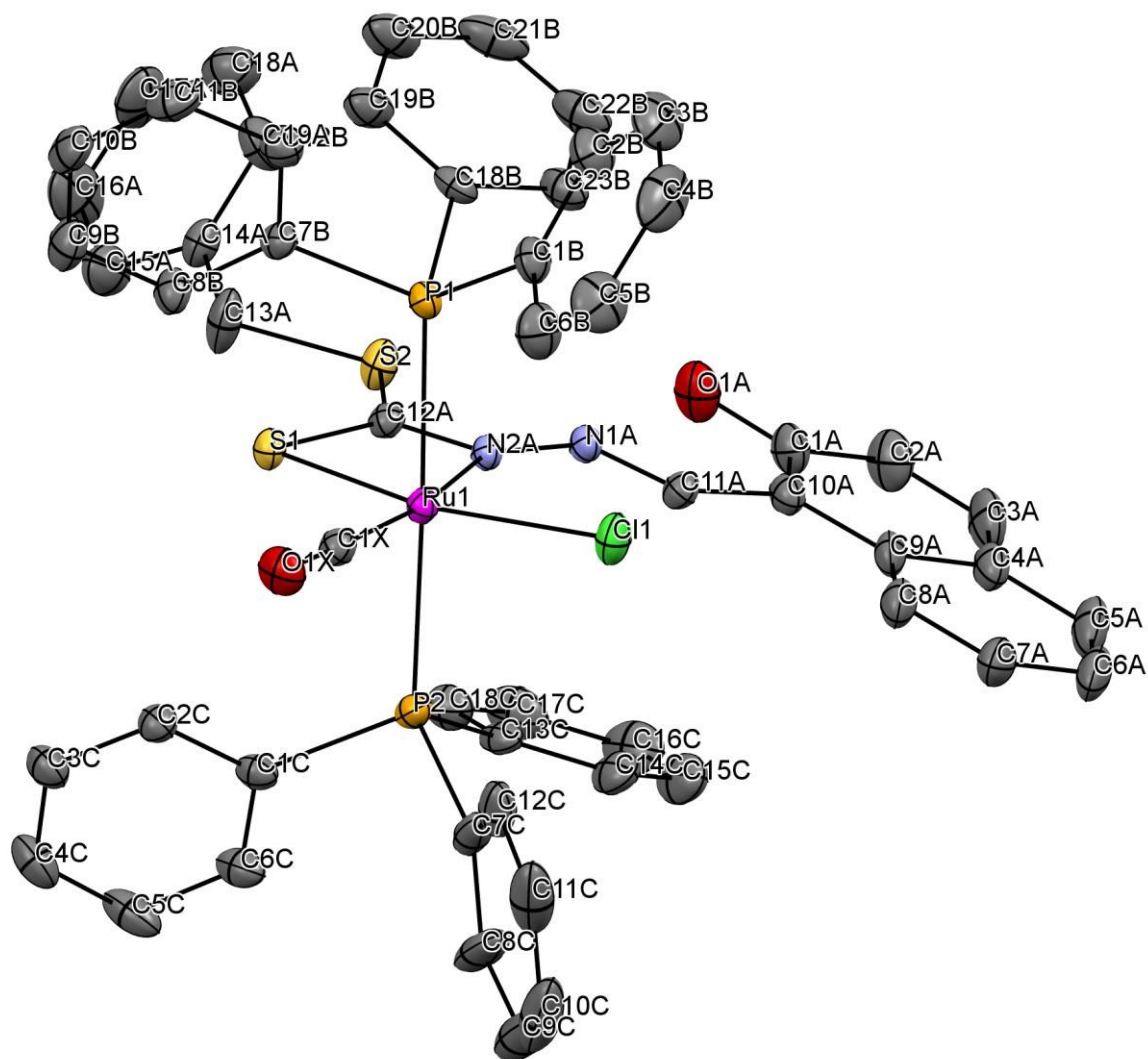


Fig. 1 ORTEP plot of complex $[\text{Ru}(\text{H-Nap-sbdtc})(\text{CO})\text{Cl}(\text{PPh}_3)_2]$ (**1**). Thermal ellipsoids are drawn at the 30% probability level. Hydrogen atoms omitted to aid in clarity.

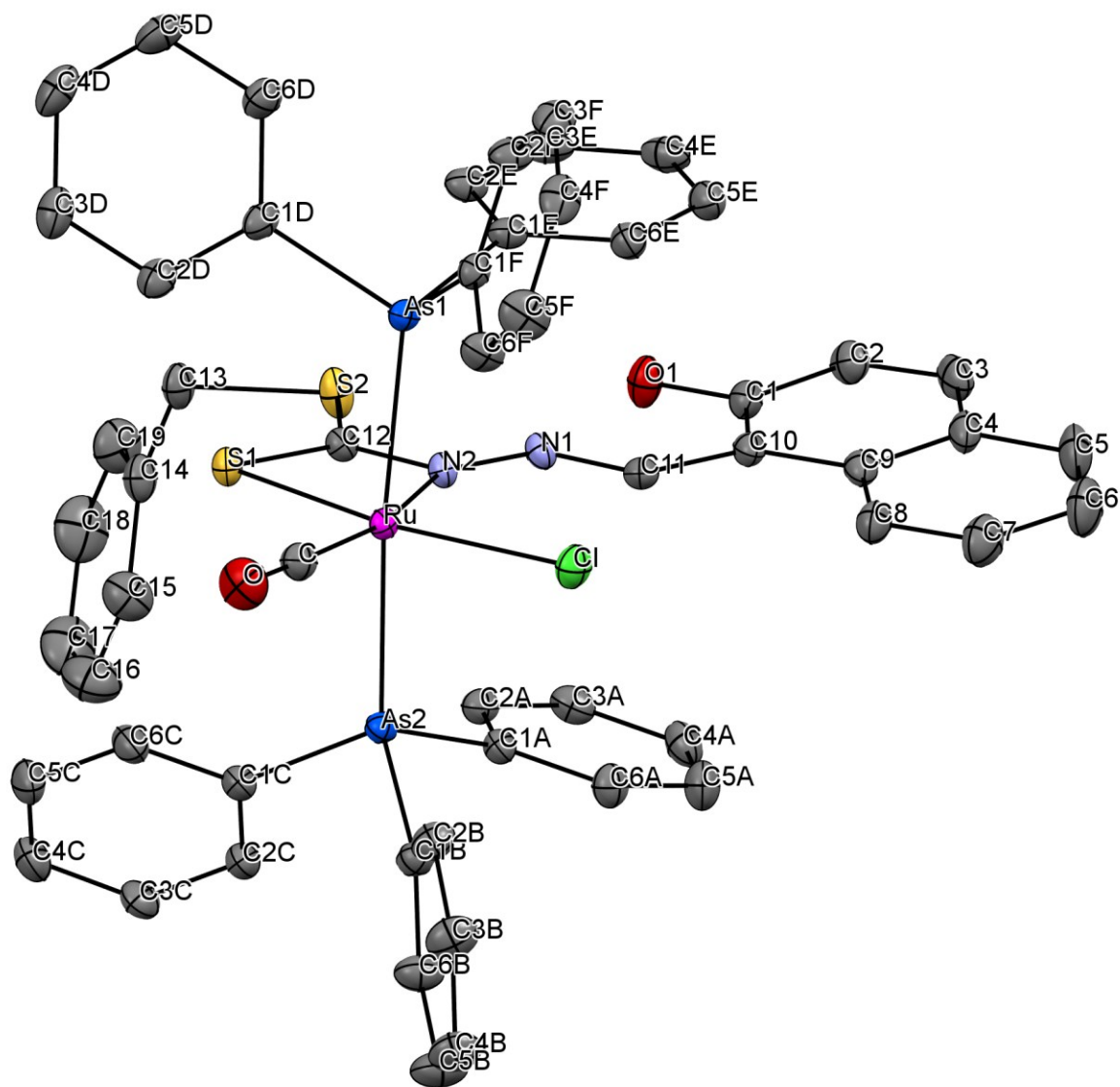


Fig. 2 ORTEP plot of complex $[\text{Ru}(\text{H-Nap-sbdtc})(\text{CO})\text{Cl}(\text{AsPh}_3)_2]$ (**2**). Thermal ellipsoids are drawn at the 30% probability level. Hydrogen atoms and the lattice chloroform molecule omitted to aid in clarity.

Table 1 Crystal data and structure refinement for complexes **1** and **2**

	1	2. CHCl₃
Identification code	Shelxl	Shelxl
Chem. formula	C ₅₆ H ₄₄ Cl N ₂ O ₂ P ₂ Ru S ₂	C ₅₇ H ₄₆ As ₂ Cl ₄ N ₂ O ₂ RuS ₂
Formula weight	1039.53	1247.79
Temperature (K)	296(2)	123(2)
Wavelength (Å)	0.71073	0.71073
Crystal system	Triclinic	monoclinic
Space group	P $\bar{1}$	P2(1)/c
Unit cell dimensions		
a (Å)	14.1173(5)	13.0014(5)
b (Å)	14.4593(8)	16.8333(6)
c (Å)	14.6783(8)	24.6941(9)
α (°)	88.900(2)	90
β (°)	71.657(2)	100.082(4)
γ (°)	85.455(2)	90
Volume (Å ³)	2835.0(2)	5321.0(3)
Z	2	4
Density (calcd) MgM ⁻³	1.218	1.558
Absorption coefficient	0.492	1.411 mm ⁻¹
F(000)	1066.0	2512
Theta range for data collection	0.970 to 31.60 °	2.986 to 41.152 °
Index ranges	-17<=h<=20 -20<=k<=21 -19<=l<=21	-23<=h<=23 -29<=k<=31 -45<=l<=40
Reflections collected	35422	67233
Independent reflections	19045 [R(int) = 0.0472]	34128 [R(int) = 0.0523]
Max. and min. transmission	0.8345 and 0.7661	1.00000 and 0.91954
Data/restraints/parameters	19045 / 0 / 619	34128 / 6 / 669
Goodness-of-fit on F ²	1.022	1.013
Final R indices [I>2sigma(I)]	R1= 0.0642, wR2= 0.1228	R1= 0.0601, wR2= 0.0939
R indices (all data)	R1= 0.1172, wR2 = 0.1499	R1= 0.1199, wR2= 0.1124

Table 2 Selected bond lengths (Å) and bond angles (°) for the complexes **1**, **2** with the optimized geometrical values

	1			2	
	X-ray data	DFT data		X-ray data	DFT data
Bond lengths (Å)					
C1X-Ru1	1.836(8)	1.854	C-Ru	1.843(2)	1.859
N2A-Ru1	2.195(6)	2.233	N2-Ru	2.1783(16)	2.194
S1-Ru1	2.390(2)	2.514	S1-Ru	2.3979(5)	2.515
Cl1-Ru1	2.406(2)	2.531	Cl-Ru	2.4301(5)	2.532
P1-Ru1	2.4642(10)	2.521	As1-Ru	2.4576(2)	2.573
P2-Ru1	2.4590(10)	2.507	As2-Ru	2.4617(3)	2.567
Bond angles (°)					
C1X-Ru1-N2A	168.0(3)	164.822	C-Ru-N2	166.22(7)	165.713
C1X-Ru1-S1	101.9(2)	98.716	C-Ru-S1	100.04(6)	99.544
N2A-Ru1-S1	66.17(16)	66.123	N2-Ru-S1	66.19(4)	66.173
C1X-Ru1-Cl1	95.5(3)	96.459	C-Ru-Cl	94.56(6)	94.946
N2A-Ru1-Cl1	96.48(16)	98.714	N2-Ru-Cl	99.21(4)	99.336
S1-Ru1-Cl1	162.42(8)	164.786	S1-Ru-Cl	165.378(18)	165.507
C1X-Ru1-P2	89.9(2)	91.260	C-Ru-As1	92.83(6)	90.15
N2A-Ru1-P2	89.27(16)	89.781	N2-Ru-As1	87.36(4)	90.055
S1-Ru1-P2	91.37(6)	90.919	S1-Ru-As1	88.835(14)	92.091
Cl1-Ru1-P2	91.22(7)	87.654	Cl-Ru-As1	89.699(14)	90.152
C1X-Ru1-P1	89.0(2)	89.969	C-Ru-As2	93.76(6)	90.43
N2A-Ru1-P1	91.60(16)	90.036	N2-Ru-As2	86.59(4)	90.305
S1-Ru1-P1	87.69(6)	92.687	S1-Ru-As2	91.458(14)	91.50
Cl1-Ru1-P1	90.09(7)	88.395	Cl-Ru-As2	88.319(14)	90.469
P2-Ru1-P1	178.34(4)	175.971	As1-Ru-As2	173.255(9)	176.21
C1B-P1-Ru1	118.1(3)	116.537	C1E-As1-Ru	110.05(5)	116.988
C7B-P1-Ru1	116.4(2)	115.633	C1F-As1-Ru	121.45(6)	114.621
C18B-P1-Ru1	113.8(2)	113.983	C1D-As1-Ru	117.10(6)	117.273
C7C-P2-Ru1	118.1(4)	117.697	C1C-As2-Ru	118.06(6)	117.221
C1C-P2-Ru1	116.0(2)	116.734	C1A-As2-Ru	110.31(6)	115.343
C13C-P2-Ru1	113.3(2)	111.969	C1B-As2-Ru	119.48(6)	116.184
C12A-S1-Ru1	82.7(3)	79.901	C12-S1-Ru	81.97(7)	79.822
O1X-C1X-Ru1	178.0(7)	175.925	O-C-Ru	178.48(19)	176.72
C12A-N2A-Ru1	100.3(4)	101.484	C12-N2-Ru	100.90(12)	101.796
N1A-N2A-Ru1	144.5(5)	141.683	N1-N2-Ru	144.08(12)	141.187

The complex **1** crystallized in the triclinic belonging to the $P\bar{1}$ space group with 2 independent molecule within the unit cell, whereas the complex **2** crystallized in the monoclinic system belonging to the space group $P 21/c$ with 4 independent molecule within the unit cell (Fig. S1). The ruthenium(II) ion exhibits a hexa coordination with an octahedral geometry, where

equatorial coordination comes from NS bidentate chelating ligand [**H₂-(Nap-sbdtc)**], a chloride, a carbonyl carbon and a pair of triphenylphosphines/triphenylarsines completes the axial coordination.³⁰ The NS chelated dithiocarbazate ligand coordinates in a bidentate manner to the ruthenium(II) ion via hydrazinic nitrogen N(2) and thiolate sulphur atom forming more strained four membered chelate ring. Formation of the four-membered chelate ring, even after removal of hydroxy group from the naphthyl ring to prevent intramolecular hydrogen bonding, points to the other possibility that steric interaction of the dithiocarbazate ligands with the PPh₃/AsPh₃ has forced them to take up such an unprecedented coordination mode.³¹ Though the PPh₃/AsPh₃ ligands usually prefer to occupy mutually *cis* position for better π -interaction, in these complexes the presence of CO a stronger π -acidic ligand, might have forced the bulky PPh₃/AsPh₃ ligands to take *trans* position for steric reasons.¹³ Ruthenium(II) ion is therefore sitting in a core RuCCINSP₂/As₂ coordination environment, which is distorted octahedral in nature as reflected in all the bond parameters around ruthenium.

In complex **1**, the ruthenium atom is in a distorted octahedral environment with *trans* angles of [P(1)–Ru(1)–P(2)] 178.34(4)^o and [Cl(1)–Ru(1)–S(1)] 101.9(2)^o. The carbonyl group *trans* to the coordinated N(2)A atom [N(2)A–Ru(1)–C(1)X] with an angle of 168.0(3). The *trans* angles deviate from linearity and N(2)A, S(1) (four membered ring) leads to small N(2)A–Ru(1)–S(1) bite angle 66.17(16)^o.^{32a} The ruthenium–ligand distances namely, Ru(1)–C(1)X 1.836(8) Å, Ru(1)–N(2)A 2.195(6) Å, Ru(1)–S(1) 2.390(2) Å, Ru(1)–Cl(1) 2.406(2) Å, Ru(1)–P(2) 2.4590(10) Å, Ru(1)–P(1) 2.4642(10) Å were found in the complexes agree well with that reported for similar other ruthenium complexes containing triphenylphosphine in *trans* position and the chlorine is *trans* to the sulfur atom.^{32b} The same prodigy occurred with technetium and rhenium complexes in different oxidation states containing same type of dithiocarbazates.^{23b} Furthermore, there exists intermolecular hydrogen bonding between OH group and N(1) hydrazinic nitrogen atom of the dithiocarbazate ligand was also found in the complex **1** (Table 3).

In complex **2**, the ruthenium atom is in a distorted octahedral environment with *trans* angles of [As(1)–Ru(1)–As(2)] 173.255(9)^o and [Cl(1)–Ru(1)–S(1)] 165.378(18)^o. The carbonyl group *trans* to the coordinated N(2)A atom [N(2)–Ru(1)–C(1)] with an angle of 166.22(7)^o. The *trans* angles deviate from linearity and N(2), S(1) (four membered ring) leads to small N(2)–Ru(1)–S(1) bite angle 66.19(4)^o.^{12,32c} The ruthenium–ligand distances namely, Ru(1)–C(1)

1.843(2) Å, Ru(1)–N(2) 2.1783(16) Å, Ru(1)–S(1) 2.3979(5) Å, Ru(1)–Cl(1) 2.4301(5) Å, Ru(1)–As(2) 2.4576(2) Å, Ru(1)–As(1) 2.4617(3) Å were found in the complexes agree well with that reported for similar other ruthenium complexes containing triphenylarsine in *trans* position and the chlorine is trans to the sulfur atom. Furthermore, there exists intermolecular hydrogen bonding between OH group and N(1) nitrogen atom (O–H...N contact) of the dithiocarbamate ligand was also found in the complex **2** (Table 3). The unit cell packing diagram of the complexes **1** and **2** along with hydrogen bonding is given in Fig. S1.

Table 3 Hydrogen bonds for the complexes **1** and **2** [Å and °]

Compound	D–H...A	d(D–H)	d(H...A)	d(D...A)	<(DHA)
1	O2–H1–N1	0.81	3.09	2.571(2)	43.9
2	O1–H1–S2	0.84	2.87	3.5841(15)	144.6
	O1–H1–N1	0.84	1.83	2.569(2)	145.8
	C11–H11A–Cl	0.95	2.59	3.494(2)	158.5
	C13–H13A–S1	0.99	2.56	3.232(2)	125.1
	C2B–H2BA–Cl	0.95	2.93	3.550(2)	124.4
	C1S–H1SA–Cl	1.00	2.83	3.662(5)	141.4

Symmetry operation: Complex **1**: 'x, y, z'; '-x, -y, -z', Complex **2**: 'x, y, z'; '-x, y+1/2'; '-z+1/2'; '-x, -y, -z'; 'x, -y-1/2'; 'z-1/2'. [D= donator, A=acceptor]

Structure of complexes **1** and **2**: Density functional theory calculations

The calculations using the density functional theory (DFT) method of GAUSSIAN-09 were carried out to obtain an insight into the bonding properties of the complexes. The initial geometries were taken from the single-crystal X-ray data of complexes **1**, **2** and subjected to optimization (Fig. S8). The geometrical parameters viz. bond lengths, bond angles and bond energies were calculated using the GAUSSIAN-09 package. Some theoretically calculated geometric parameters were collected in Table 2 and the general trends observed in the experimental data are reproduced in the calculations. The calculated and experimental values of bond angles are reasonably close. A correlation to some extent between the HOMO–LUMO energy gap of a complexes and its chemical reactivity is expected. This is because the chemical reactivity is related to chemical hardness, defined as the resistance to perturbation in the electron

distribution in a molecule. Contour plots of molecular orbitals of the complexes were generated using Gauss view 9.0 and the frontier molecular orbitals in 1–4 were calculated (Fig. 3). Positive and negative regions are shown in red and blue colors respectively.

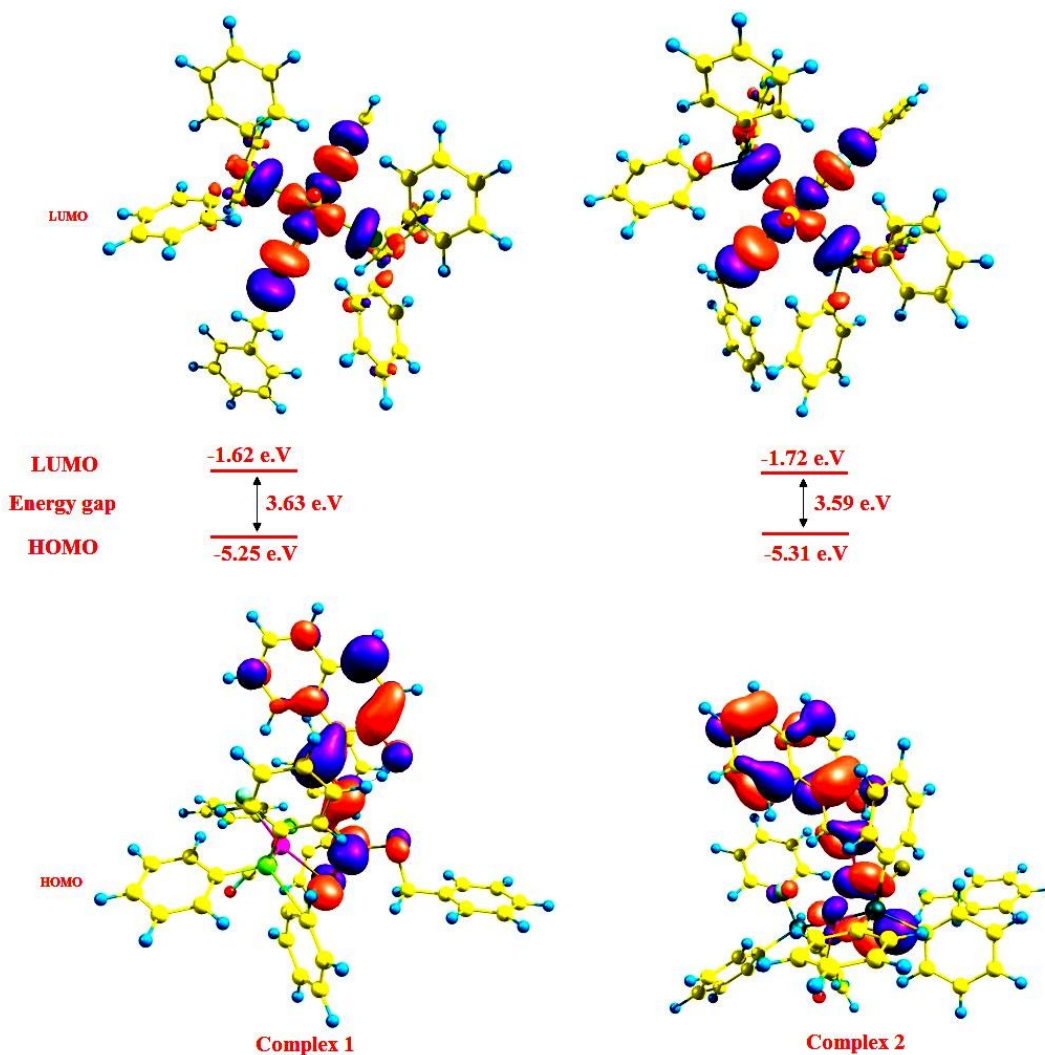


Fig. 3 Frontier molecular orbitals of complexes **1**, **2** and their HOMO–LUMO energy gaps.

It is seen that the complexes **1** and **2**, the electron density of the HOMO is localized largely on naphthyl ring, sulphur atoms in the ligand [H₂-(Nap-sbdtc)] and lesser extent on the metal ion without relevant contributions, while in the LUMO major contributions from in the metal ion and to a lesser extent from dithiocarbazate ligand and PPh₃/AsPh₃ rings.^{33a} So the electron transfer occurs from the highest occupied molecular orbital (HOMO) to lowest unoccupied molecular orbital (LUMO), it can be inferred that the electron transfer in complexes

is related to LMCT. These transition from HOMO to LUMO explains the first allowed excitation. The calculated HOMO energies of the complexes vary as **1** (-5.25) < **2** (-5.31) and those of LUMO exhibit a similar trend: **1** (-1.62) < **2** (-1.72). The HOMO–LUMO energy gaps in complex **1** (3.63 eV) and **2** (3.59 eV) are almost the same, which is consistent with the experimentally observed order of biologic efficiencies of complexes. The calculated atomic charge and electron configurations of donor and ruthenium center atoms were listed in Table 4.

Table 4 Charges (a.u.) and electron configurations for the complexes **1** and **2**

Atom	Complex 1		Complex 2	
	Charge	Natural electronic configuration	Charge	Natural electronic configuration
Ru	-0.219	[core]5s(0.37)4d(7.70) 5p(0.59)5d(0.02)6p(0.28)	-0.441	[core]5s(0.39)4d(7.74)5p(0.92)5d(0.02)6p(0.01)
P/As	0.723	[core]3s(1.15)3p(2.65)4p(0.02)	0.901	[core]4s(1.18)4p(2.36)5p(0.02)
P/As	0.727	[core]3s(1.15)3p(2.65)4p(0.02)	0.897	[core]4s(1.18)4p(2.36)5p(0.02)
Cl	-0.365	[core]3s(1.87)3p(5.53)	-0.319	[core]3s(1.87)3p(5.53)
S	0.123	[core]3s(1.69)3p(4.22)4p(0.01)	0.104	[core]3S(1.69)3p(4.23)4p(0.01)
C	0.044	[core]2s(1.09)2p(2.13) 3s(0.02)3p(0.03)	0.077	[core]2s(1.09)2p(2.12)3s(0.02)3p(0.03)

According to this table, the electron populations on s and p orbitals of oxygen, nitrogen and sulfur donor atoms in both complexes are less than the expected values of valence orbitals, while the computed electron population in central ion in both complexes is more than the expected value in Ru⁺² with d⁶ electronic configuration. The calculated formal charge on the ruthenium ion (**1** = -0.219; **2** = -0.441) in the complexes were lower than the formal charge +2, that confirming a significant charge donation from the ligands. This confirms the electron transmission of donor atoms toward the central metal. The calculated electronic configurations (Table 4) of the donor atoms with reference to s and p orbitals are consistent with electron donation towards the ruthenium ion.^{33b, c}

DNA interaction studies

DNA binding by fluorescence spectra

The investigation of the binding of metal complexes to DNA is of prime importance in the development of anticancer drugs. This technique is commonly used to study potential interactions (and their likely nature) between DNA and metal complexes. The emissive titration studies have been performed by monitoring the changes in emission intensity by aliquot addition of DNA.³⁴ Usually, intercalation between the metal complexes and DNA results in hypochromism with or without red/blue shift; on the other hand, non-intercalative/electrostatic interaction causes hyperchromism. From the emissive titration spectra (Fig. 4),

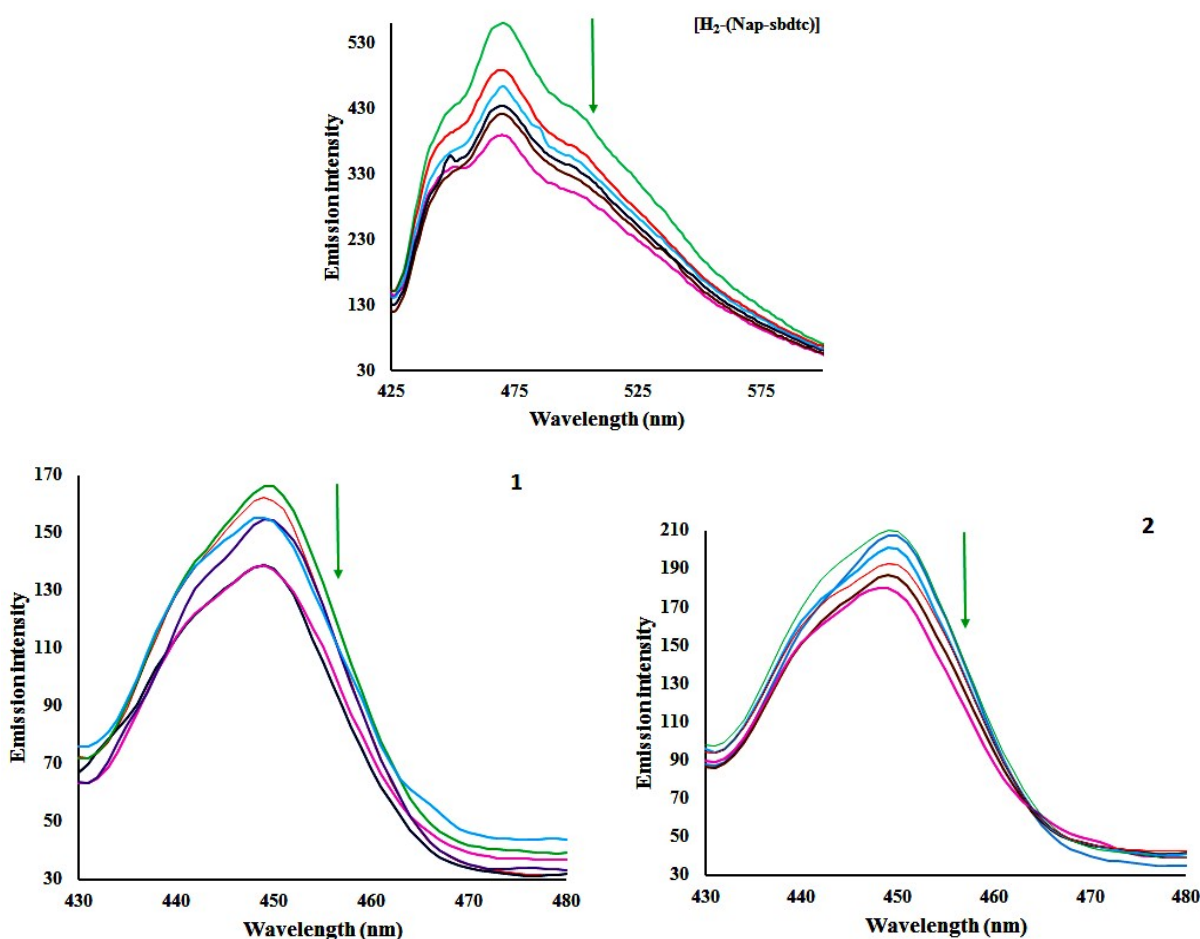


Fig. 4 Emissive titration of the compounds $[\text{H}_2\text{-(Nap-sbdtc)}]$, **1** and **2** ($50 \mu\text{M}$) with CT-DNA ($0\text{-}50 \mu\text{M}$). Arrows indicate increasing amounts of DNA concentration.

it is apparent that upon addition of increasing concentration of CT-DNA ($0\text{-}50 \mu\text{M}$) to a solution of $\text{H}_2\text{-(Nap-sbdtc)}$ displayed hypochromism (43.82%) at 472 nm along with a small red shift ($\sim 2 \text{ nm}$). The complexes **1** and **2** show different behavior relative to those of ligand. The complexes **1**

and **2** exhibited the band at 450 nm showed hypochromism of about 27.06 and 17.03% with a small red shift (~ 2 nm). The observed hypochromism is due to an intercalative mode of binding involving a strong stacking interaction between extending aromaticity of ligand and the base pairs of DNA. The hypochromism is commonly consistent with the strength of intercalative interaction. The intensity of bands decreased from the original intensities based on the DNA binding enhancement. In order to further elucidate affinity of the tested compounds towards CT DNA quantitatively, the intrinsic binding constant (K_b) has been determined using the following Scatchard equation.³⁵

$$C_F = C_T [(I/I_0) - P] / [1 - P]$$

where, C_T is the concentration of the probe (complex) added; C_F is the concentration of the free probe, and I_0 and I were its emission intensities in the absence and in the presence of DNA, respectively. P is the ratio of the observed emission quantum yield of the bound probe to the free probe. The value of P was obtained from a plot of I/I_0 versus $1/[DNA]$ such that the limiting emission yield is given by the y -Intercept. The amount of bound probe (C_B) at any concentration was equal to $C_T - C_F$. The obtained Scatchard plots of r/C_F versus r for tested compounds with increasing concentration of CT-DNA were depicted in Fig. 5.

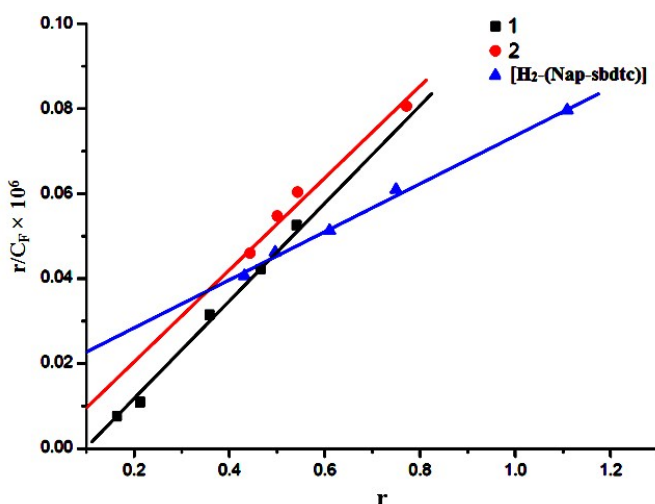


Fig. 5 Scatchard plots of r/C_f Vs r for compounds [H_2 -(Nap-sbdtc)], **1** and **2** with increasing concentration of CT-DNA.

Table 5 CT-DNA binding constant (K_b), quenching constant (K_q) and apparent binding constant (K_{app}) values

Compound	K_b (M^{-1})	K_q (M^{-1})	K_{app} (M^{-1})
[H_2 -(Nap-sbdtc)]	5.69×10^4	5.36×10^3	4.02×10^5
1	1.21×10^5	7.89×10^3	5.90×10^5
2	9.38×10^4	5.90×10^3	4.42×10^5

A plot of r/C_F versus r ($= C_B/ [DNA]$) give the intrinsic binding constant (K_b) values. It has been found that the intrinsic binding constant (K_b) values for the interaction of, **H_2 -(Nap-sbdtc)**, **1** and **2** with CT-DNA were listed in Table 5. The results derived from the emissive titration experiments suggest that all the compounds (**H_2 -(Nap-sbdtc)**, **1** and **2**) can bind to DNA. However the complexes interact with CT-DNA more strongly than the corresponding ligand.³⁶ The K_b values suggested that the DNA-binding affinities of the compounds follow the order **1** > **2** > **H_2 -(Nap-sbdtc)**. For intercalative ligand with an extended aromatic plane and good conjugation effects from substituted group can greatly enhance the DNA-binding ability of the ruthenium(II) complexes.

Ethidium bromide displacement study

To gain deep insight into interaction of the ligand and their ruthenium(II) complexes to bind CT-DNA was studied by evaluating the fluorescence emission intensity of the ethidium bromide (EB)-DNA system upon the addition of different amounts of the selected compounds. EB is a DNA intercalating agent that fluoresces when bound to the polynucleotide molecule (actually the fluorescence intensity of EB increases by almost 20-fold after binding to DNA).³⁷ The fluorescence of EB increases after intercalating into DNA. If the metal complexes intercalate into DNA, it leads to a decrease in the binding sites of DNA available for EB resulting in decrease in the fluorescence intensity of the EB-DNA system.^{38a} The fluorescence intensity of EB-DNA decreases rapidly with increasing concentrations of the compounds. This illustrates that, as the concentration of the ligand and complexes **1** and **2** increases, the emission band at 604 nm for EB exhibited hypochromism up to 45.51, 71.43 and 78.64% with slight red/blue shift from the initial fluorescence intensity respectively. Results depicted in Fig. 6 underlined that the ligand and their

ruthenium(II) complex efficiently quenched the fluorescence emission of EB. Notably, the fluorescence quenching constant evaluated using the Stern–Volmer equation.^{38b}

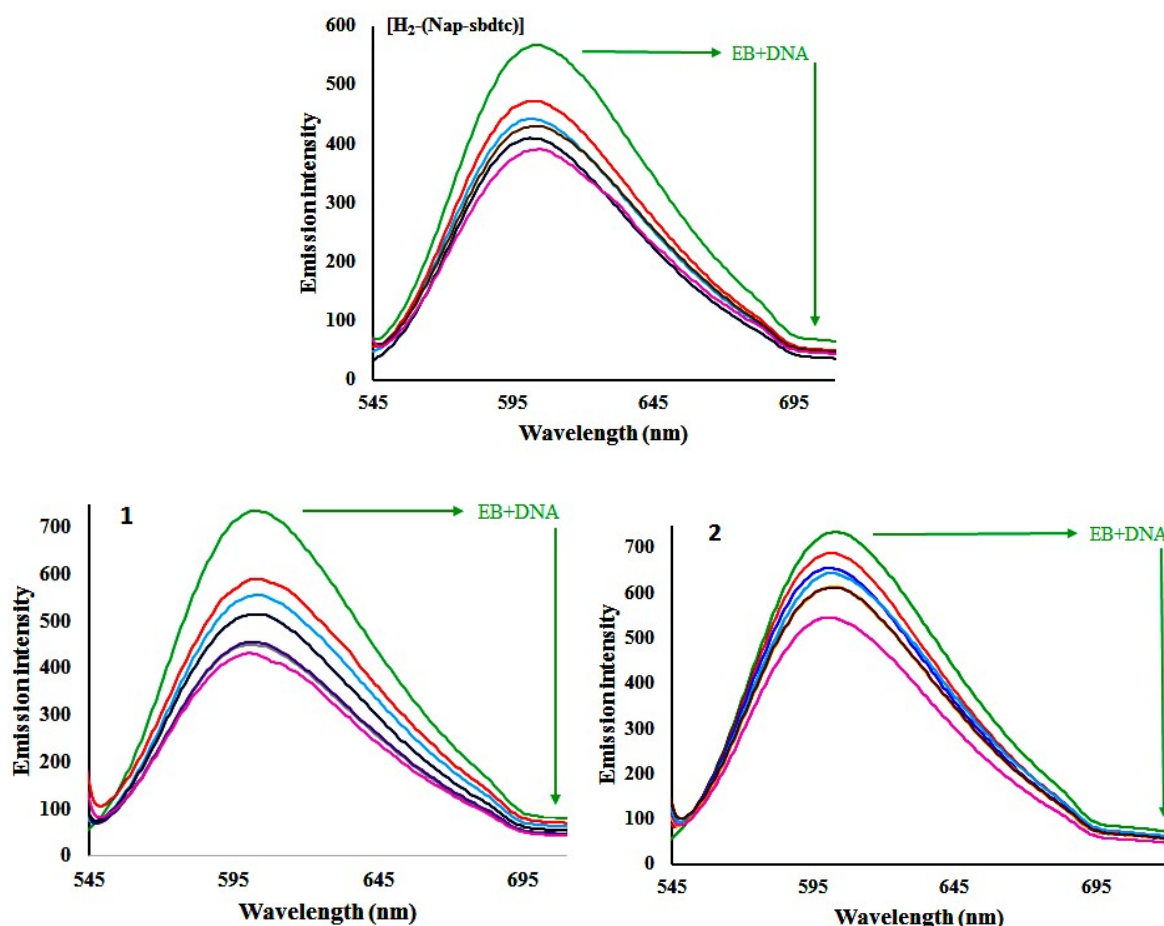


Fig. 6 Steady-state fluorescence spectra of the compounds [$\text{H}_2\text{-(Nap-sbdtc)}$], **1** and **2** (0–50 μM) with EB bound CT-DNA (7.5 μM). The arrows show diminution of the emission intensity with increasing concentration of compounds.

$$F_0/F = 1 + K_q [Q]$$

where F_0 and F are the fluorescence intensities in the absence and the presence of the quencher, respectively. K_q is the linear Stern–Volmer quenching constant. The K_q value is obtained with a slope from the plot of F_0/F versus $[Q]$. The Stern–Volmer plots of F_0/F versus $[Q]$ was shown in Fig. 7. The quenching constant (K_q) values were obtained from the slope, thus indicating that the complexes strongly bind to DNA. The quenching constant (K_q) values were obtained from the

slope, which was 5.36×10^3 , 7.89×10^3 , 5.90×10^3 for the ligand and their complexes **1**, **2** respectively.

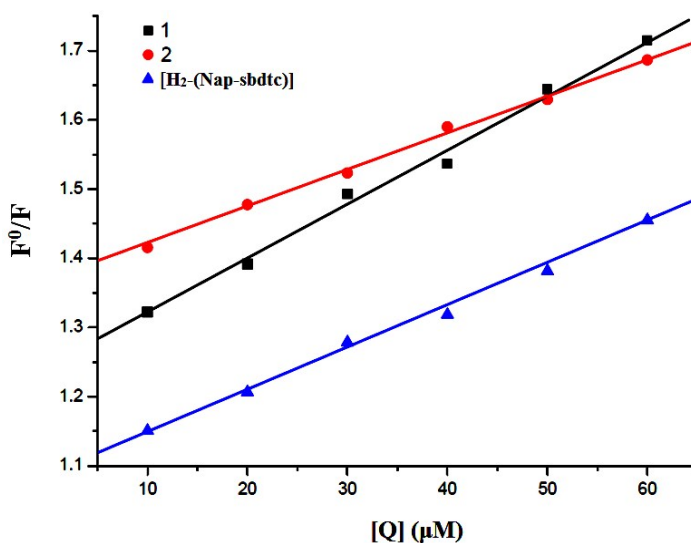


Fig. 7 Stern–Volmer plots of fluorescence titration of compounds [**H₂-(Nap-sbdtc)**], **1** and **2** with CT-DNA.

The selected test compounds can quench the EB emission by either competing with EB for binding sites or by accepting the excited state photon. It is unlikely that the ligand and their ruthenium complexes can compete with EB for intercalative binding sites. Further the apparent DNA binding constant (K_{app}) values were also calculated using the following equation^{38c}

$$K_{EB} [EB] = K_{app} [M_{50\%}]$$

where, $K_{EB} = 1.0 \times 10^7 \text{ M}^{-1}$ is the DNA binding constant of EB; [EB] is the concentration of EB ($7.5 \mu\text{M}$) and $[M_{50\%}]$ is the concentration of the compound used to obtain 50% reduction in fluorescence intensity of DNA pretreated with EB. The K_{app} value for ligand and their complexes **1** and **2** were given in Table 5. The DNA binding ability of the compounds follows the order **1** > **2** > **H₂-(Nap-sbdtc)**, which is consistent with the results obtained from above fluorescence spectral studies.³⁹ The quenching and binding constants of the ligand and the ruthenium(II) complexes suggested that the interaction of the tested compounds with CT-DNA should be of intercalation.

Viscosity measurement

To clarify the nature of the interaction between the compounds and CT-DNA, viscosity measurements were performed. These measurements provide sensitive detection of the binding mode of the present compounds. Hydrodynamic measurements that are sensitive to changes in length (i.e., viscosity and sedimentation) are regarded as the least ambiguous and the most critical tests of a binding model in solution in the absence of crystallographic or NMR structural data.^{40, 41} In general, the viscosity of CT-DNA increases when a compound binds DNA in an intercalating mode but remains unchanged when a compound binds DNA in an electrostatic mode. If the groove binding mode occurs, there is a little effect on the viscosity of DNA. The length of the DNA helix increases upon intercalation as base pairs are separated to accommodate the binding ligand, which results in the increased viscosity of the DNA. The viscosity measurements of compounds on the relative viscosities of CT-DNA were shown in Fig. 8.

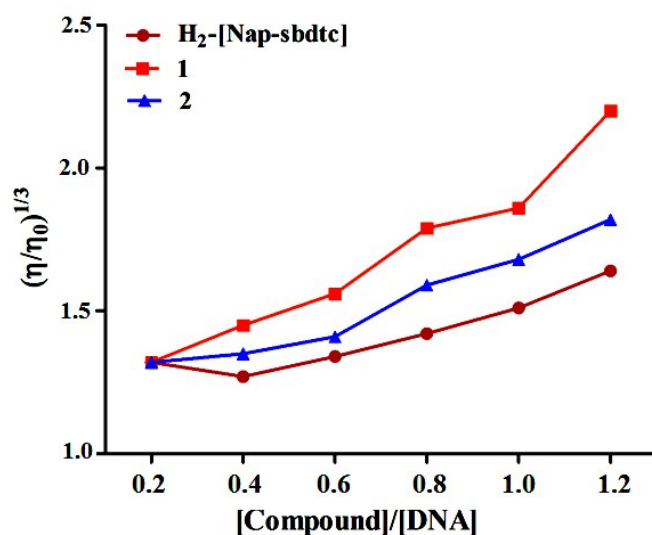


Fig. 8 Effect of the compounds ($[\text{H}_2\text{-(Nap-sbdtc)}]$, **1** and **2**) on the viscosity of CT DNA.

When ligand and their ruthenium(II) complexes **1**, **2** were treated with CT-DNA (200 μM) and the concentrations of ruthenium complexes (0-120 μM) are increased from a ratio of $R = 0-1.2$ ($1/R = [\text{Ru}]/[\text{DNA}]$), the relative viscosity of DNA increases steadily in the order $\mathbf{1} > \mathbf{2} > \text{H}_2\text{-(Nap-sbdtc)}$. The selected compounds which contain planar ligands, can deeply intercalate into DNA base pairs and increase DNA viscosity similar to some known intercalators indicative of a classical intercalation.⁴² This results are consistent with our above mentioned hypothesis.

Nuclease activity

The nuclease activity of ruthenium(II) complexes was investigated by the electrophoretic mobility shift assay using supercoiled plasmid DNA. This method is commonly used to study the DNA cleavage activity of metal complexes. This can be achieved by monitoring the transition from the naturally occurring, covalently closed circular form (Form I) to the open circular relaxed form (Form II). This occurs when one of the strands of the plasmid is nicked, and can be determined by gel electrophoresis of the plasmid.^{43, 24} Extended irradiation results in a buildup of nicks on both strands of the plasmid, which eventually results in its opening to the linear form (Form III). Hence, uncut plasmids (Form I) will appear to migrate more rapidly than the same plasmid when linearized (Form III). Moreover, the nicked circles (Form II), which are the bulkiest, will be the slowest migrating species in the gel (since the separation is not only by charge but also by size).^{44a} As mentioned in the above introduction, the ability of the ruthenium(II)–Schiff base complexes to cleave DNA was assayed with the aid of gel electrophoresis on pBR322 DNA as the substrate in the medium of 5 mM tris-(hydroxymethyl)aminomethane (Tris)-HCl/50mM NaCl buffer (pH-7.2) in the absence of external additives. The DNA was mixed with fixed concentrations (25 μ M) of ligand and their ruthenium(II) complexes and was incubated at 37 $^{\circ}$ C for 4 h (Fig. 9).

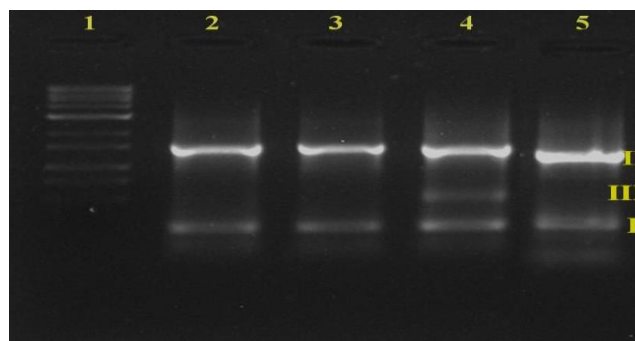


Fig. 9 Agarose gel electrophoresis images of supercoiled pBR322 DNA incubated for 4 h at 37 $^{\circ}$ C with fixed concentration of compounds. Lane 1: DNA ladder, Lane 2: DNA control, Lane 3: DNA+ [H₂-(Nap-sbdtc)] (25 μ M), Lane 4: DNA+ Complex 1 (25 μ M), Lane 5: DNA+ Complex 2 (25 μ M).

Moreover control experiments performed using DNA alone (Lane 2) and ligand (Lane 3) in separate lanes did not reveal any apparent cleavage of DNA. From Lane 4 and 5, the fixed concentration of the complexes (25 μ M), convert SC DNA (Form I) into NC DNA (Form II).^{44b} In addition the linear form (Form III) obtained from the cleavage of SC DNA (Form I). The

complexes did not require any addition of external agents to affect DNA cleavage activity. As depicted in Fig.9 the complexes **1** and **2** exhibited more effective DNA cleavage activity than ligand under the identical experimental conditions.

Protein interaction studies (BSA)

Fluorescence spectra

Interaction between the most abundant blood proteins, which is serum albumin (BSA/HSA), and metal complexes have attracted immense current interest because of their structural homology with human serum albumin. It constitutes about 55% of total plasma proteins and plays a pivotal role in the transport of drug and their metabolism.⁴⁵ It exhibits intrinsic fluorescence because of the presence of aromatic amino acids phenylalanine, tyrosine, and tryptophan. If the tyrosine is ionized, then its fluorescence is completely quenched, whereas phenylalanine has a very low quantum yield. This means that intrinsic fluorescence of BSA is due to tryptophan alone. The relative ratio of fluorescence intensity for three amino acids (tryptophan, tyrosine and phenylalanine) residues is 100:9:0.5, and thus the intrinsic fluorescence intensity of BSA when excited at 295 nm mainly comes from the tryptophan residues such as Trp-134 and Trp-212 more exposed to the environment.⁴⁶ Therefore, fluorescence behavior of BSA can provide significant information about the structure, dynamics, and protein folding. A solution of BSA (5 mM) was titrated with various concentrations of the compounds **H₂-(Nap-sbdtc)**, **1** and **2** (0-50 mM) in the range of 230-530 nm (λ_{exc} 280 nm). Fig. 10 showed that the effect of increasing concentration of compounds on the fluorescence emission of BSA.

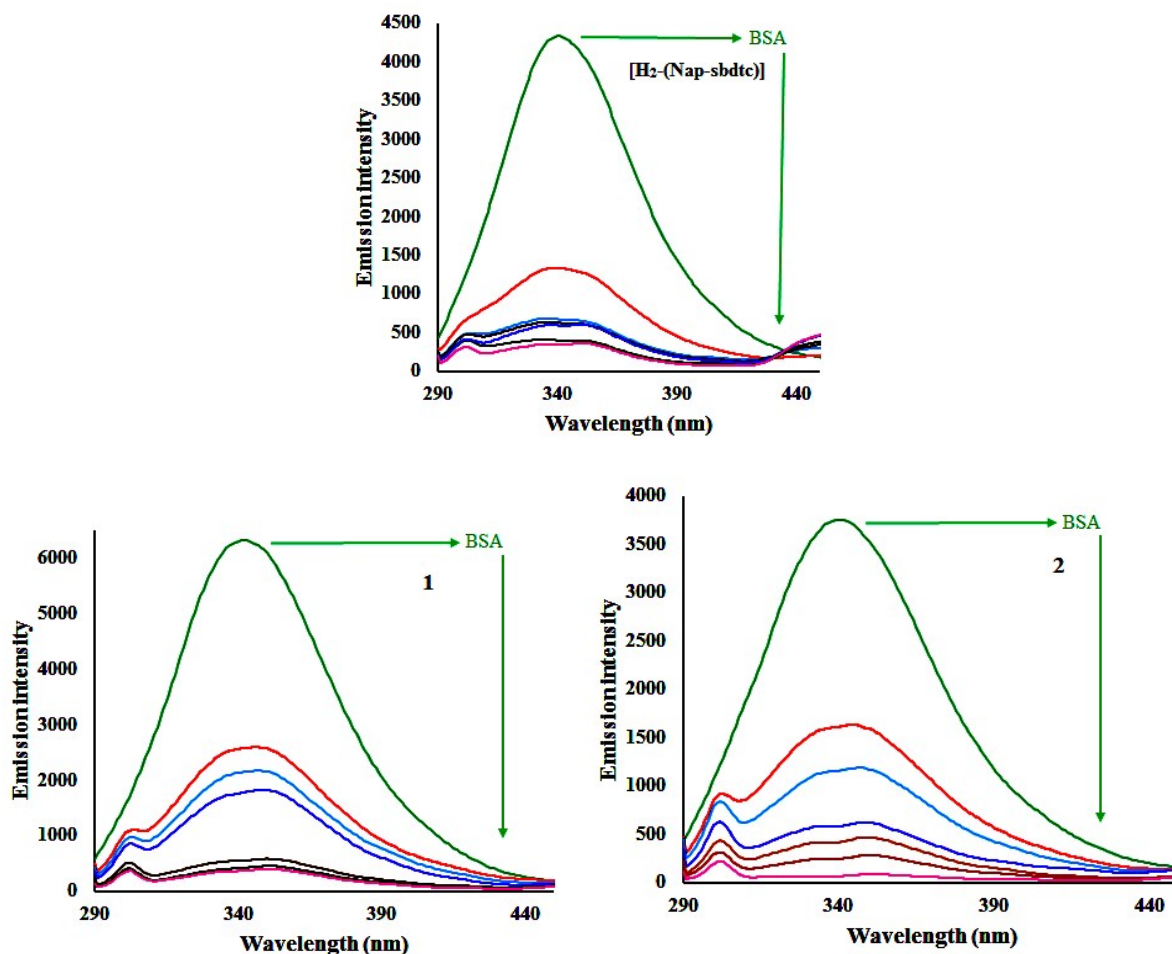


Fig. 10 Fluorescence titrations of the compounds $[\text{H}_2\text{-(Nap-sbdtc)}]$, **1** and **2** (0–50 μM) with BSA (1 μM). The arrows show diminution of the emission intensity with increasing concentration of compounds.

An examination of the spectra showed a noteworthy decrease in fluorescence intensity at ~ 343 nm between the test compounds and BSA protein. The observed red shift is mainly due to the fact that the active site in protein is buried in a hydrophobic environment. It suggested that some interaction is taking place between the complexes and the BSA protein. To have a deep insight into the quenching progression, quenching constant (K_q) was evaluated following Stern-Volmer and Scatchard equation.⁴⁷

$$\text{Log } [I_0 - I / I] = \text{log } K_{\text{bin}} + n \text{ log } [Q]$$

where, K_{bin} is the binding constant of the compound with BSA and n is the number of binding sites. The number of binding sites (n) and the binding constant (K_{bin}) have been found from the plot of $\log (I_0-I) / I$ versus $\log [Q]$ (Fig. 11).

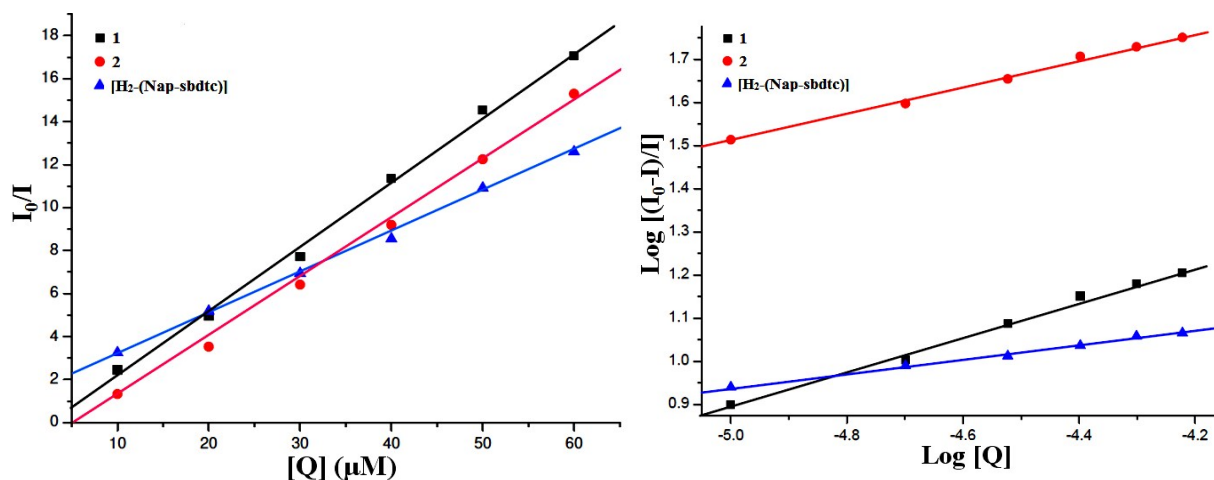


Fig. 11 Stern-Volmer plots and Scatchard plots of the fluorescence titration of the compounds [H_2 -(Nap-sbdtc)], **1** and **2** with BSA.

Table 6 Quenching constant (K_q), binding constant (K_{bin}), and number of binding sites (n) for the interactions of complexes with BSA

Compound	K_q (M^{-1})	K_{bin} (M^{-1})	'n' value
[H_2 -(Nap-sbdtc)]	1.84×10^5	2.95×10^5	0.94
1	3.03×10^5	4.43×10^5	1.12
2	3.62×10^5	1.53×10^6	1.66

The calculated K_q , K_{bin} , and n values are given in Table 6. The value of 'n' indicates the existence of a single binding site in BSA for the complexes or ligand.¹³ The larger values of K_q and K_{bin} indicate a strong interaction between the BSA protein and the complexes over the ligand used in this study. The DNA binding ability of the compounds follows the order **2** > **1** > H_2 -(Nap-sbdtc), which is consistent with the results obtained from above binding affinity studies.

UV-Vis spectral study

The fluorescence quenching mechanisms are usually classified as either static or dynamic quenching. Static quenching usually results from the formation of a complex between quencher and fluorophore in the ground state, whereas in dynamic quenching the fluorophore and quencher get in touch with each other during the transient existence of the excited state.^{48a} One can have an idea about the type of quenching from UV-Vis absorption spectral studies. UV-Vis spectra of BSA in presence of compounds displayed (Fig. 12) an increase in absorption intensity of the BSA suggesting static interaction due to formation of ground state complex as reported earlier.^{48b}

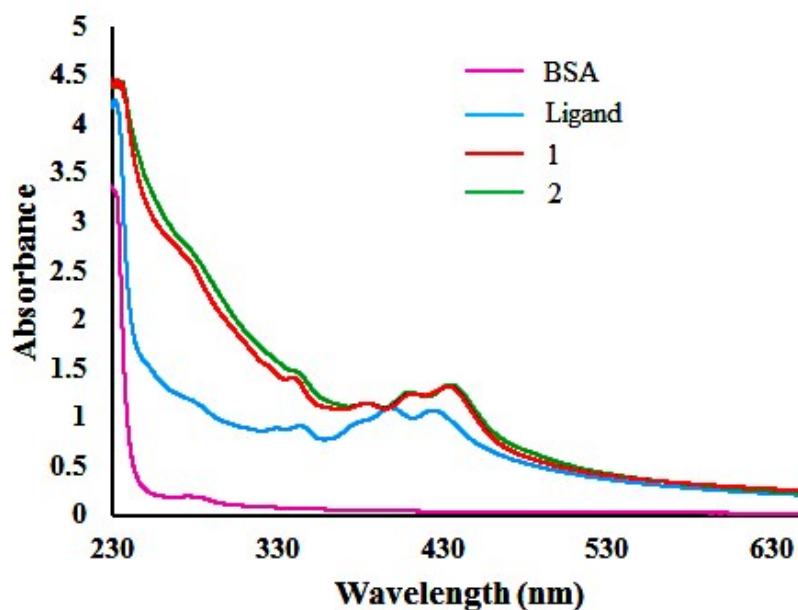


Fig. 12 Absorbance titrations of the compounds [$\text{H}_2\text{-(Nap-sbdtc)}$], **1** and **2** with BSA.

Protein cleavage study

In order to access the ability of the ligand and their complexes **1** and **2** serve as a synthetic metallo proteases, the BSA photocleavage activity of the compounds was studied using 4 mM BSA in 50 mM Tris-HCl buffer staining with CBR-250 at room temperature. The extent of protein photocleavage for fixed concentration of the compounds (50 μM) was compared with the untreated BSA band.⁴⁹ As depicted in Fig. 13,

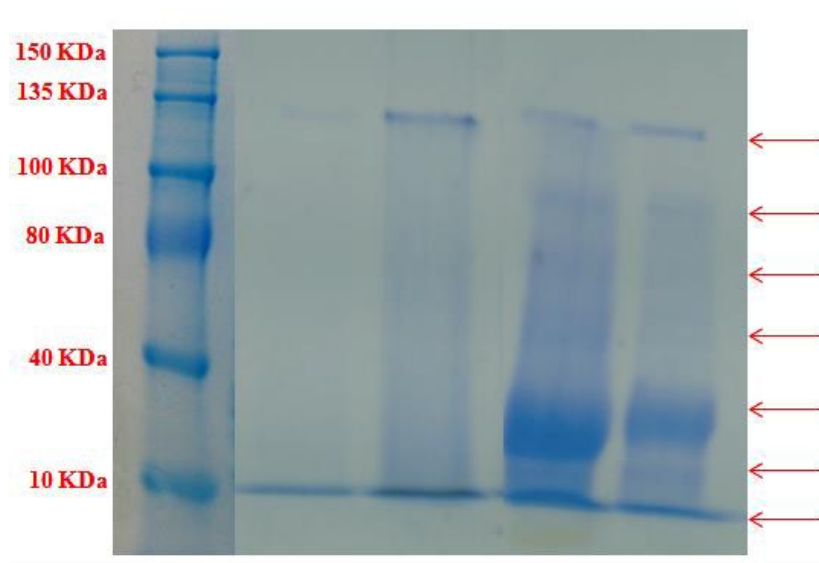


Fig. 13 SDS page diagram for the cleavage of BSA (4 mM) incubated for 4 h at 37 °C with fixed concentration of compounds. Lane 1: Molecular marker, Lane 2: BSA control, Lane 3: [H₂-(Nap-sbdtc)]+BSA (50 mM), Lane 4: Complex 1+ BSA (50 mM), Lane 5: Complex 2+ BSA (50 mM).

the SDS-PAGE gel diagrams was observed that BSA alone and ligand (Lane 2 and 3) did not show any apparent cleavage under these same experimental conditions whereas the complexes **1** and **2** (Lane 4 and 5) with BSA display more electrophoretic bands corresponding to protein fragments of 20 kDa, 60 kDa, 100 kDa and 120 kDa. The complexes **1** and **2** showed significant smearing or fading of the BSA band indicating photocleavage of BSA.⁵⁰ Among them, the fading of band suggested that non-specific binding of the complexes to BSA, leading to cleavage into very small fragments, which is supported by BSA binding studies as reported earlier.

Anticancer activity *in vitro*

Cancer cell growth inhibition

The antiproliferative activities of ligand and their complexes **1**, **2** were appraised against normal Vero cell line and human cervical carcinoma cell line (HeLa) using MTT assay. Cisplatin was used as positive control to assess the cytotoxicity of the test compounds.^{51a} The results were analyzed by cell viability curves and expressed with IC₅₀ values in the studied concentration range from 5 to 50 μM. The IC₅₀ values obtained are summarized in Table 7 and Fig.14.

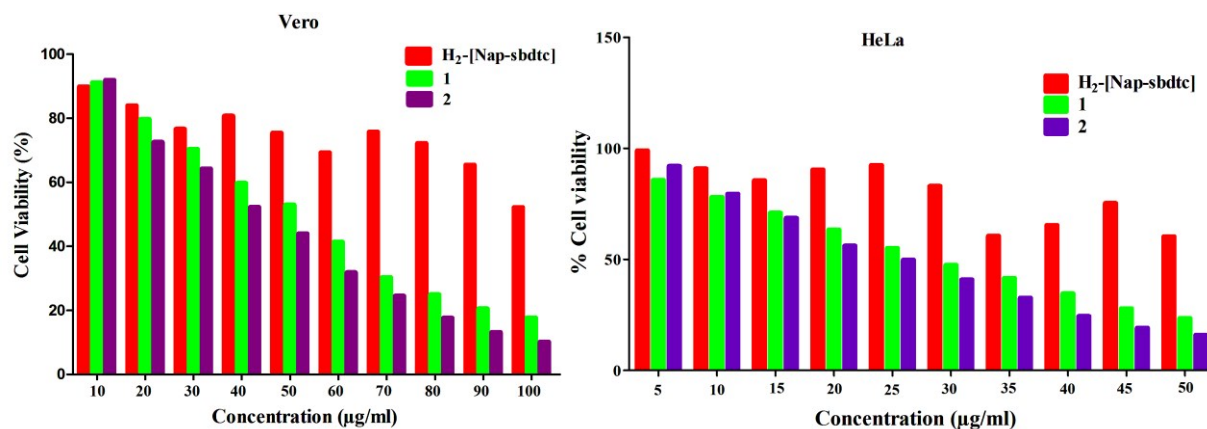


Fig. 14 Cytotoxicity of the compounds $[H_2-(Nap-sbdtc)]$, **1** and **2** after 24 h of incubation on Vero and HeLa cell lines.

Table 7 *In vitro* cytotoxicity of the compounds in Vero and HeLa cancer cell lines

Compound	IC_{50} (μM) ^a	
	Vero	HeLa
$[H_2-(Nap-sbdtc)]$	>100	>100
1	47.37 \pm 1.32	26.42 \pm 2.37
2	39.33 \pm 1.05	22.91 \pm 1.85
Cisplatin ^b	---	13.00 \pm 2.01

^aFifty percent inhibitory concentration after exposure for 48 h in the MTT assay.

^bData from Ref. [51].

The amount of cell proliferation significantly decreased in a dose-dependent manner on supplementation with compounds, as observed within 24 h of incubation against HeLa/Vero cells under identical experimental conditions. The ligand is not significantly active against (HeLa/Vero) cells, in contrast to the complexes (Table 7). The ruthenium complexes exhibited higher cytotoxicity *in vitro* against the selected cell lines than cisplatin, which is a widely used clinical antitumor drug in the low micro molar concentration.^{51b} This is due to the fact that ruthenium complexes have a capacity to reduce the energy status in tumors as well as to enhance tumor hypoxia, which also influences their antitumor activities. It is known that naphthalene ring compartment ligand-containing ruthenium complexes have a wide range of biological activities such as antitumor, apoptosis and interaction with DNA inhibiting replication, transcription and

other nuclear functions and arresting cancer cell proliferation so as to arrest tumor growth.⁵² The results indicate these complexes have beneficial features for potential anticancer agents.

Morphological changes in AO/EB and DAPI fluorescence study

Apoptotic pathways are important targets that should be considered in the design of potential anticancer agents. It is especially advantageous if the new compound triggers the death of cancer cells by apoptosis. Apoptosis induction is an anti-proliferative mechanism by which the cancer cells undergo programmed death. Cells undergoing apoptosis are characterized by several morphological and biochemical changes including cell shrinkage, chromatin condensation and DNA fragmentation.⁵³ Apoptotic cells exhibit increased plasma membrane permeability to certain fluorescent dyes ex: AO/EB, Hoechst, AO/PI, DAPI etc. In this study, we used AO/EB and DAPI staining assay. The cytological changes were observed in the treated cells are classified into four types on the basis of the fluorescence emission and morphological features of chromatin condensation in the AO/EB stained nuclei: (i) Viable cells, which have highly organized nuclei, fluoresce green; (ii) early apoptotic cells, which show nuclear condensation, emit orange-green fluorescence; (iii) in late apoptotic cells with highly condensed or fragmented chromatin the nuclei fluoresce orange to red; and (iv) necrotic cells fluoresce orange to red with no indication of chromatin fragmentation.⁵⁴ All these morphological changes were observed after treatment of the cancer cells with the complexes. To investigate the morphological changes AO/EB and DAPI fluorescence staining was performed and resulting images of the control and treated HeLa cells are depicted in Fig. 15.

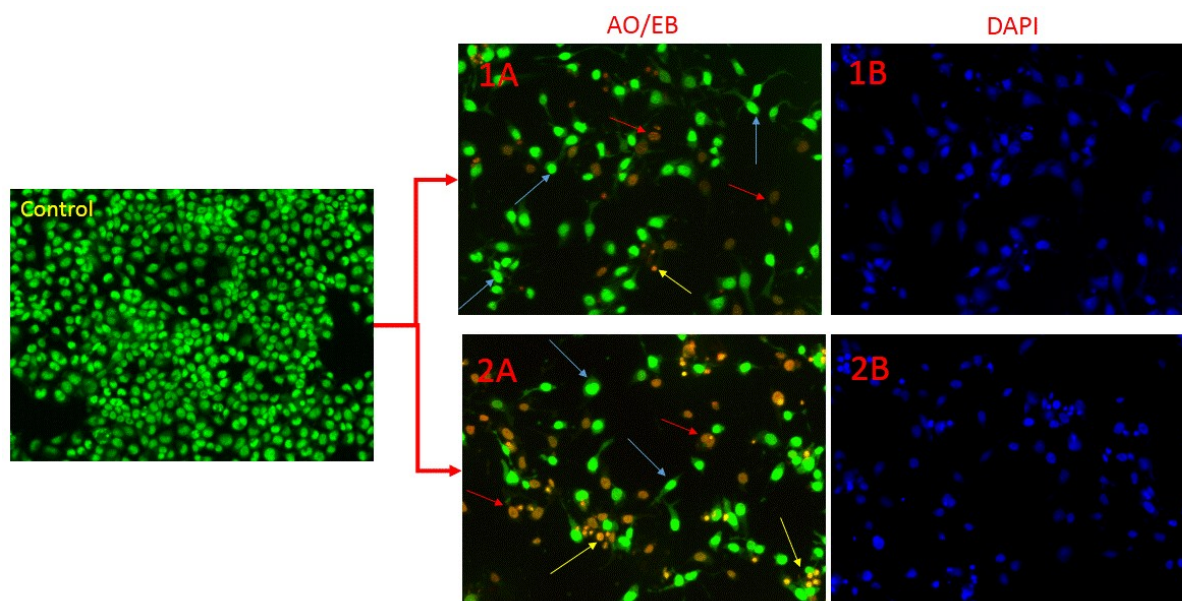


Fig. 15 AO/EB (1A, 2A) and DAPI (1B, 2B) stained HeLa cells at 24 h incubation by the treatment of complexes **1** and **2**. The yellow, blue and red arrows show early apoptotic cells with blebbing, late apoptosis and necrotic cells respectively.

In this figure yellow arrows show early apoptotic HeLa cells with membrane blebbing which is seen at fixed concentration of the complexes **1**, **2** and blue arrows exhibit late apoptotic cells with chromatin aggregation, that is, highly condensed chromatin. Necrotic cells have a uniform orange to red nuclei with condensed structure were observed.¹² Overall results indicate that complexes **1** and **2** induced cell death by necrosis in good agreement with the above toxicity results.

Conclusion

Two new organo-ruthenium(II) complexes of 2-hydroxy-1-naphthaldehyde-S-benzylthiocarbamate have been synthesized and characterized by various spectral techniques. The characterization of the ruthenium(II) complexes was accomplished by analytical and spectral (IR, UV-vis, NMR, ESI-MS) methods. The solid state structure of the two complexes was confirmed by single-crystal X-ray crystallography. Interestingly, the S-benzylthiocarbamate coordinated as NS fashion through the hydrazinic nitrogen and thiolate sulfur by forming four-membered chelate ring. The XRD study also reveals the presence of a distorted octahedral geometry around the ruthenium(II) ion. The structural parameters of the complexes that are in good agreement with

X-ray analysis were obtained by DFT calculations. Complex **2**, which has the lowest energy gap between the HOMO and LUMO. Various physico-chemical techniques demonstrated that these complexes effectively bind with DNA through intercalative interactions. The gel electrophoresis assay demonstrated that the complexes have been found to promote the cleavage ability of the pBR322 plasmid DNA. In addition, the binding ability to BSA proteins has also been explored to be a static one, which is the requisite for a drug to act as an anticancer agent. Moreover, they all exhibit significant cytotoxic activity towards normal Vero cell line and HeLa cancer cell lines and the characteristics of apoptosis in cell morphology have been observed by AO/EB and DAPI staining.

Acknowledgments

The authors Dr. P.V. and P.V gratefully acknowledge UGC [F.No.40-66/2011 (SR)] for financial support. The author (R.N) thankful to DST for financial assistance (Project No.SR/FT/CS-95/2010). The authors would like to thank the director, CAS in botany, School of life sciences, University of Madras for providing laboratory facilities to perform the cell lines studies.

Electronic supplementary information (ESI) available:

Packing diagram for complexes **1** and **2** (Fig. S1), UV-vis and Emission spectra of compounds (Fig. S2), representative NMR (^1H , ^{13}C and ^{31}P) spectra of complexes (Fig. S3-S6), ESI-MS spectrum of complex (Fig. S7) and optimized structure of complexes (Fig. S8). CCDC reference numbers 986059 and 985979 for complexes 1, 2. For ESI and crystallographic data in CIF or other electronic format see DOI:

References

1. (a) N. P. E. Barry, P. J. Sadler, *Chem. Commun.* 2013, **49**, 5106–5131. (b) B. W. Harper, A. M. Krause-Heuer, M. P. Grant, M. Manohar, K. B. Garbutcheon-Singh, J. R. Aldrich-Wright, *Chem. Eur. J.* 2010, **16**, 7064–7077. (c) N. J. Wheate, S. Walker, G. E. Craig, R. Oun, *Dalton Trans.* 2010, **39**, 8113–8127.
2. L. Breydo, V. N. Uversky, *Metallomics*, 2011, **3**, 1163–1180.
3. N. P. E. Barry, P. J. Sadler, *Chem. commun.* 2013, **49**, 5106–5131.
4. P. C. A. Bruijninx, P. J. Sadler, *Curr. Opin. Chem. Biol.* 2008, **12**, 197–206.
5. (a) G. Suess-Fink, *Dalton Trans.* 2010, **39**, 1673–1688. (b) A. C. G. Hotze, B. M. Kariuki, M. J. Hannon, *Angew. Chem.* 2006, **118**, 4957–4960.
6. (a) W. H. Ang, P. J. Dyson, *Eur. J. Inorg. Chem.* 2006, **20**, 4003–4018. (b) P. Schluga, C. G. Hartinger, A. Egger, E. Reisner, M. Galanski, M. A. Jakupec, B. K. Keppler, *Dalton Trans.* 2006, 1796–1802. (c) D. Wang, S. J. Lippard, *Nature Rev. Drug Discovery* 2005, **4**, 307–320. (d) P. J. Dyson, *Chimia* 2007, **61**, 698–703. (e) E. R. Jamieson, S. J. Lippard, *Chem. Rev.* 1999, **99**, 2467–2498.
7. A. R. Timerbaev, C. G. Hartinger, S. S. Aleksenko and B. K. Keppler, *Chem. Rev.*, 2006, **106**, 2224–2248.
8. M. R. Maurya, A. Kumar, A. R. Bhat, A. Azam, C. Bader, D. Rehder, *Inorg. Chem.* 2006, **45**, 1260–1269.
9. M. Akbar Ali, A. H. Mirza, R. J. Fereday, R. J. Butcher, J. M. Fuller, S. C. Drew, L. Gahan, G. R. Hanson, B. Moubaraki, K. S. Murray, *Inorg. Chim. Acta* 2005, **358**, 3937–3948.
10. N. Bharti, R. Maurya, F. Naqvi, A. Bhattacharya, S. Bhattacharya, A. Amir, *Eur. J. Med. Chem.* 2000, **35**, 481–486.
11. R. Takjoo, M. Yazdanbakhsh, A. A. Kaju, Y. Chen, *Chin. J. Chem.*, 2010, **28**, 221–228.
12. P. Vijayan, P. Viswanathamurthi, V. Silambarasan, D. Velmurugan, K. Velmurugan, R. Nandhakumar, R. J. Butcher, T. Silambarasan, R. Dhandapani, *J. Organomet. Chem.*, 2014, **768**, 163–177.
13. a) G. Sethuraman, B. M. Yamin, M. Shamsuddin, A. Usman, I. Abdul Razak, H. K. Fun, *Acta Cryst.* (2002). **E58**, o649–o651.

- b) N. Ahmed, J. J. Levison, S. D. Robinson and M. F. Uttley, *Inorg. Synth.*, 1974, **15**, 45–64.
14. SMART & SAINT Software Reference manuals, version 5.0, Bruker AXS Inc., Madison, WI, 1998.
15. G.M. Sheldrick, SHELXL97, *Program for Crystal Structure Refinement*, University of Gottingen, Germany, 1997.
16. M. J. Frisch, G. W. Trucks, H. B. Schlegel, G. E. Scuseria, M. A. Robb, J. R. Cheeseman, G. Scalmani, V. Barone, B. Mennucci, G. A. Petersson, H. Nakatsuji, M. Caricato, X. Li, H. P. Hratchian, A. F. Izmaylov, J. Bloino, G. Zheng, J. L. Sonnenberg, M. Hada, M. Ehara, K. Toyota, R. Fukuda, J. Hasegawa, M. Ishida, T. Nakajima, Y. Honda, O. Kitao, H. Nakai, T. Vreven, J. A. Montgomery, J. E. Peralta, F. Ogliaro, M. Bearpark, J. J. Heyd, E. Brothers, K. N. Kudin, V. N. Staroverov, T. Keith, R. Kobayashi, J. Normand, K. Raghavachari, A. Rendell, J. C. Burant, S. S. Iyengar, J. Tomasi, M. Cossi, N. Rega, J. M. Millam, M. Klene, J. E. Knox, J. B. Cross, V. Bakken, C. Adamo, J. Jaramillo, R. Gomperts, R. E. Stratmann, O. Yazyev, A. J. Austin, R. Cammi, C. Pomelli, J. W. Ochterski, R. L. Martin, K. Morokuma, V. G. Zakrzewski, G. A. Voth, P. Salvador, J. J. Dannenberg, S. Dapprich, A. D. Daniels, O. Farkas, J. B. Foresman, J. V. Ortiz, J. Cioslowski, D. J. Fox, Gaussian 09, Inc., Wallingford CT, 2010.
17. E. Reed, L.A. Curtiss, F. Weinhold, *Chem. Rev.* 1988, **88**, 899–926.
18. A. C. G. Hotze, E. P. L. van der Geer, S. E. Caspers, H. Kooijman, A. L. Spek, J. G. Haasnoot and J. Reedijk, *Inorg. Chem.*, 2004, **43**, 4935–4943.
19. (a) R. Loganathan, S. Ramakrishnan, E. Suresh, A. Riyasdeen, M.A. Akbarsha, M. Palaniandavar, *Inorg. Chem.*, 2012, **51**, 5512–5532. (b) U.K. Laemmler, *Nature*, 1970, **227**, 680–685.
20. T. Mosmann, *J. Immunol. Methods*, 1983, **65**, 55–63.
21. M. Ali, A. Mirza, R. Butcher, M. Tarafder, B. Tan, A. Ali, *J. Inorg. Biochem.* 2002, **92**, 141–148.
22. P. Kalavani, R. Prabhakaran, P. Poornima, F. Dallemer, K. Vijayalakshmi, V. Vijayapadma, K. Natarajan, *Organometallics*, 2012, **31**, 8323–8332.
23. a) R. Ramachandran, G. Prakash, S. Selvamurugan, P. Viswanathamurthi, J.G. Malecki, V. Ramkumar, *Dalton Trans.* 2014, **43**, 7889–7902.

- b) A. Marchi, R. Rossi, L. Magon, A. Duatti, R. Pasqualini, V. Ferretti, V. Bertolasi, *J. Chem. Soc., Dalton Trans.*, 1990, 1411-1416.
24. P. Kalaivani, R. Prabhakaran, E. Vaishnavi, T. Rueffer, H. Lang, P. Poornima, R. Renganathan, V. VijayaPadmad, K. Natarajan, *Inorg. Chem. Front.*, 2014, **1**, 311–324.
25. (a) M. I. Bruce, J. Howard, I. W. Nowell, G. Shaw and P. Woodward, *J. Chem. Soc., Chem. Commun.* 1972, 1041–1042; (b) D. Pandiarajan, R. Ramesh, *J. Organomet. Chem.* 2013, **723**, 26–35.
26. D. Senthil Raja, G. Paramaguru, N. S. P. Bhuvanesh, J. H. Reibenspies, R. Renganathan, K. Natarajan, *Dalton Trans.*, 2011, 4548–4559.
27. P. Kalaivani, R. Prabhakaran, F. Dallemer, P. Poornima, E. Vaishnavi, E. Ramachandran, V. Vijaya Padma, R. Renganathan, K. Natarajan, *Metallomics*, 2012, **4**, 101–113.
28. N. Chitrapriya, T.S. Kamatchi, M. Zeller, H. Lee, K. Natarajan, *Spectrochim. Acta A*, 2011, **81**, 128–134.
29. T. Sathiyakamatchi, N. Chitrapriya, H. Lee, C.F. Fronczek, F.R. Fronczek, K. Natarajan, *Dalton Trans.* 2012, **41**, 2066–2077.
30. J.G. Malecki, A. Maron, M. Serda, J. Polanski, *Polyhedron*, 2013, **56**, 44–54.
31. R. Prabhakaran, P. Kalaivani, S. V. Renukadevi, R. Huang, K. Senthilkumar, R. Karvembu, K. Natarajan, *Inorg. Chem.* 2012, **51**, 3525–3532.
32. (a) F. Basuli, S.M. Peng, S. Bhattacharya, *Inorg. Chem.* 2000, **39**, 1120–1127. (b) F. Basuli, S.-M. Peng and S. Bhattacharya, *Inorg. Chem.*, 2001, **40**, 1126–1133. (c) R. Prabhakaran, P. Kalaivani, R. Huang, M. Sieger, W. Kaim, P. Viswanathamurthi, F. Dallemer and K. Natarajan, *Inorg. Chim. Acta*, 2011, **376**, 317–324.
33. (a) M. Ganeshpandian, R. Loganathan, E. Suresh, A. Riyasdeen, M. A. Akbarsha, M. Palaniandavar, *Dalton Trans.*, 2014, **43**, 1203-1219. (b) P. Paul, R. J. Butcher, S. Bhattacharya, *Inorg. Chim. Acta*, 2015, **425**, 67–75. (c) S. K. Sarkar, M. S. Jana, T. K. Mondal, C. Sinha, *Appl. Organometal. Chem.* 2014, **28**, 641–651.
34. C. Shobha Devi, D. Anil Kumar, Surya S. Singh, N. Gabra, N. Deepika, Y. Praveen Kumar, S. Satyanarayana, *Eur. J. Med. Chem.* 2013, **64**, 410–421.
35. Q. Yu, Y. Liu, J. Zhang, F. Yang, D. Sun, D. Liu, Y. Zhou, J. Liu, *Metallomics*, 2013, **5**, 222–231.
36. M. Asadi, E. Safaei, B. Ranjbar, L. Hasani, *New J. Chem.* 2004, **28**, 1227–1234.

37. J. B. Lepecq, C. J. Paoletti, *J. Mol. Biol.* 1967, **27**, 87–106.
38. (a) B. C. Baguley and M. LeBret, *Biochemistry*, 1984, **23**, 937–943. (b) T. B. Wyman, F. Nicol, O. Zelphati, P. V. Scaria, C. Plank, F. C. Szoka, *Biochemistry*, 1997, **36**, 3008–3017. (c) J. R. Lakowicz and G. Webber, *Biochemistry*, 1973, **12**, 4161–4170.
39. J. M. Ruso, D. Attwood, M. García, P. Taboada, L. M. Varela, V. Mosquera, *Langmuir*, 2001, **17**, 5189–5195.
40. E. J. Gabbay, R. E. Scofield, C. S. Baxter, *J. Am. Chem. Soc.* 1973, **95**, 7850–7857.
41. P. R. Reddy, A. Shilpa, N. Raju, P. Raghavaiah, *J. Inorg. Biochem.*, 2011, **105**, 1603–1612.
42. D. Lahiri, S. Roy, S. Saha, R. Majumdar, R. R. Dighe, A. R. Chakravarty, *Dalton Trans.*, 2010, **39**, 1807–1816.
43. K. Ghosh, P. Kumar, V. Mohan, U. P. Singh, S. Kasiri, S. S. Mandal, *Inorg. Chem.*, 2012, **51**, 3343–3345.
44. (a) G. Süß-Fink, *Dalton Trans.*, 2010, **39**, 1673–1688. (b) P. U. Maheswari, S. Roy, H. den Dulk, S. Barends, G. van Wezel, B. Kozlevcar, P. Gamez, J. Reedijk, *J. Am. Chem. Soc.* 2006, **128**, 710–711.
45. Y. Zhang, Z. D. Qi, D. Zheng, C. H. Li and Y. Liu, *Biol. Trace Elem. Res.*, 2009, **130**, 172–184.
46. C. V. Dang, R. F. Ebert, W. R. Bell, *J. Biol. Chem.*, 1985, **260**, 9713–9719.
47. J.R. Lakowicz, Principles of Fluorescence Spectroscopy, *Kluwer Academic/ Plenum Press*, New York, 1999.
48. (a) S. M. T. Shaikh, J. Seetharamappa, S. Ashoka, P. B. Kandagal, *Dyes Pigm.*, 2007, **73**, 211–216. (b) D. Senthil Raja, N. S. P. Bhuvanesh and K. Natarajan, *Eur. J. Med. Chem.*, 2011, **46**, 4584–4594.
49. V. Rajendiran, R. Karthik, M. Palaniandavar, H.S. Evans, V.S. Periasamay, M.A. Akbarsha, B.S. Srinag, H. Krishnamurthy, *Inorg. Chem.* 2007, **46**, 8208–8221.
50. N. H. Khan, N. Pandya, N. C. Maity, M. Kumar, M. Rajesh, P. R. I. Kureshy, S. H. R. Abdi, S. Mishr, S. Das, H. C. Bajaj, *Eur. J. Med. Chem.* 2011, **46**, 5074–5085.
51. (a) P. Krishnamorthy, P. Sathyadevi, A.H. Cowlwy, R.R. Butorac, N. Dharamaraj, *Eur. J. Med. Chem.*, 2011, **46**, 3376–3387. (b) T.S. Kamatchi, N. Chitrapriya, H. Lee, C.F. Fronczek, F.R. Fronczek, K. Natarajan, *Dalton Trans.*, 2012, **41**, 2066–2077.

52. S. Tardito, C. Isella, E. Medico, L. Marchiò, E. Bevilacqua, M. Hatzoglou, O. Bussolati, R. Franchi-Gazzola, *J. Biol. Chem.* 2009, **284**, 24306-24319.
53. D. Baskic, S. Popovic, P. Ristic and N. N. Arsenijevic, *Cell Biol. Int.*, 2006, **30**, 924–932.
54. H. L. Chan, D. L. Ma, M. Yang, C. M. Che, *ChemBioChem*, 2003, **4**, 62–68.